2003

Modeling δ18O in precipitation over the tropical Americas: 1. Interannual variability and climatic controls

M. Vuille
Raymond S Bradley, *University of Massachusetts - Amherst*
M. Werner
R. Healy
F. Keimig

Modeling $\delta^{18}O$ in precipitation over the tropical Americas: 1. Interannual variability and climatic controls

M. Vuille,[1] R. S. Bradley,[1] M. Werner,[2] R. Healy,[3] and F. Keimig[1]

Received 27 December 2001; revised 27 August 2002; accepted 17 December 2002; published 18 March 2003.

[1] We use two atmospheric general circulation models (AGCMs), the ECHAM-4 and the GISS II models, to analyze the interannual variability of $\delta^{18}O$ in precipitation over the tropical Americas. Several different simulations with isotopic tracers forced with observed global sea surface temperatures (SST) between 1950 and 1998 reveal the influence of varying temperature, precipitation amount, and moisture source contributions on the predicted $\delta^{18}O$ distribution. Observational evidence from climatic (NCEP-NCAR) and sparse stable isotope (IAEA-GNIP) data is used to evaluate model performance. The models capture the essential features of surface climate over the tropical Americas in terms of both their spatial and temporal characteristics. Using a low-resolution model (GISS II), adjusted to provide a more realistic Andean topography, or a higher-resolution model (ECHAM-4 T106) leads to an improved $\delta^{18}O$ distribution over the tropical Americas with an altitude effect comparable to observations. Water vapor transport and gradual rainout and increasingly depleted composition of water vapor along its trajectory are correctly simulated in both models, although the ECHAM model appears to underestimate the continentality effect over the Amazon basin. A significant dependence of $\delta^{18}O$ on the precipitation amount is apparent in both models, in accordance with observations, while the influence of temperature seems to be less significant in most regions and is accurately reproduced by the ECHAM model only. Over most regions, however, the $\delta^{18}O$ signal in precipitation is influenced by a combination of factors, such as precipitation amount, temperature, moisture source variability, and atmospheric circulation changes. Over parts of the tropical Americas, the $\delta^{18}O$ signal is therefore also significantly correlated with ENSO because ENSO is an integrator of many factors affecting the $\delta^{18}O$ composition of precipitation. *INDEX TERMS:* 1620 Global Change: Climate dynamics (3309); 3337 Meteorology and Atmospheric Dynamics: Numerical modeling and data assimilation; 9360 Information Related to Geographic Region: South America; 4215 Oceanography: General: Climate and interannual variability (3309); *KEYWORDS:* GCM (general circulation model), ice cores, stable isotopes, South America, ENSO

Citation: Vuille, M., R. S. Bradley, M. Werner, R. Healy, and F. Keimig, Modeling $\delta^{18}O$ in precipitation over the tropical Americas: 1. Interannual variability and climatic controls, *J. Geophys. Res.*, *108*(D6), 4174, doi:10.1029/2001JD002038, 2003.

1. Introduction

[2] Stable water isotopes $H_2{}^{18}O$ and HDO in meteoric waters (rain and snow) reveal a close relationship with certain climatic parameters such as air temperature or amount of precipitation. *Dansgaard* [1964] first described a strong spatial correlation between surface temperature and $\delta^{18}O = \{[(^{18}O/^{16}O)_{sample}/(^{18}O/^{16}O)_{SMOW}] - 1\} \times 1000$, expressed in permil, where SMOW stands for standard mean ocean water. This relationship has since been used to extract paleoclimatic information from records of past precipitation preserved in ice cores, groundwater, speleothems, fluid inclusions, lake sediments, etc. While the link between the isotopic signature of the precipitation and climate is in general quite well established in polar regions, this is much less the case in midlatitudes and the tropics. As shown by *Rozanski and Araguás-Araguás* [1995] and others, the seasonal cycles of temperature (albeit very weak) and $\delta^{18}O$ composition of precipitation in the tropics are often opposed to each other, that is, high (low) temperatures coincide with more depleted (enriched) $\delta^{18}O$ values. This phenomenon is usually interpreted in the sense that the $\delta^{18}O$ composition of precipitation reflects precipitation amount rather than temperature, because at low latitudes high temperatures and rainy season tend to coincide. This ''amount effect'' is caused by the small-scale vertical convection associated with precipitation in the tropics. As condensation proceeds, the isotopically enriched molecules are preferentially removed, leaving the isotopic composition of the remaining vapor increasingly lighter. The stronger the convective nature of a particular rainfall event, the higher the total amount of precipitation and thus the more depleted

[1]Climate System Research Center, Department of Geosciences, University of Massachusetts, Amherst, Massachusetts, USA.
[2]Max Planck Institute for Biogeochemistry, Jena, Germany.
[3]Woods Hole Oceanographic Institution, Woods Hole, Massachusetts, USA.

0148-0227/03/2001JD002038$09.00

the isotopic composition of this rainwater. As oceanic air masses move inland and lose water through precipitation, the remaining atmospheric water vapor therefore becomes progressively depleted in heavy isotopes ("continentality effect"). Once the water vapor reaches an orographic obstacle, the adiabatic cooling and precipitation associated with rising air masses ("altitude effect") will further contribute to the depletion of this air mass [e.g., *Grabczak et al.*, 1983; *Gonfiantini et al.*, 2001].

[3] The isotopic composition of precipitation can also shift due to a change of the dominant source regions for precipitation at a given site [e.g., *Charles et al.*, 1994; *Cole et al.*, 1999] or because of a change in the seasonality of precipitation. The climatic signal recorded in a paleoarchive of ancient precipitation only represents the climate situation during the precipitation event itself. If during the past, the seasonality of precipitation was different (i.e., different seasonal distribution of the precipitation), this might have caused a significant shift of the isotopic signal, even though the mean annual temperature or snowfall amount might have remained the same [*Steig et al.*, 1994; *Krinner et al.*, 1997; *Werner et al.*, 2000a].

[4] Despite all the uncertainty about what might have caused past variability in stable isotopic records at low latitudes, these records are usually interpreted in a way similar to those from high latitudes, that is, as a proxy for local air temperature [e.g., *Thompson et al.*, 2000]. Clearly, there is a need to improve the interpretation of tropical paleorecords, but there is also an inadequate understanding of what controls the modern spatiotemporal pattern and variability of $\delta^{18}O$ in precipitation at low latitudes. Unfortunately, the observational data in the International Atomic Energy Agency-Global Network of Isotopes in Precipitation (IAEA-GNIP) database is rather sparse and most of the available records are very short. An analysis of the $\delta^{18}O$-climate relationship for a given region will thus always be incomplete if it is based on observational evidence alone, because of inadequate data coverage, but even more so because the different factors acting upon the $\delta^{18}O$ composition cannot be individually accounted for. Atmospheric general circulation models (AGCMs), which include stable isotopic tracers, however, are able to capture the essential physical mechanisms behind the fractionation processes of $\delta^{18}O$ in precipitation [*Jouzel et al.*, 1991, 1996, 2000; *Cole et al.*, 1993, 1999; *Joussaume and Jouzel*, 1993; *Hoffmann and Heimann*, 1997; *Hoffmann et al.*, 1998, 2000; *Werner et al.*, 2000b; *Werner and Heimann*, 2002]. Every process in the AGCM that transports water between grid boxes is extended in the isotopic tracer model to transport the water isotope tracers as well. When the transport involves a change of phase, the model uses isotopic fractionation equations to distribute the isotopes between the phases. The model transports the water isotopes between atmospheric grid boxes and among the surface reservoirs with the same processes used to transport regular water. Isotopic fractionation, including both equilibrium and kinetic effects, is accounted for at every change of phase, that is, surface evaporation, condensation, and reevaporation or falling precipitation.

[5] Here we present results from several AGCM experiments using the NASA-GISS II and ECHAM-4 models under varying modern boundary conditions. We limit our analysis to $\delta^{18}O$, although the models are also capable of simulating the stable isotopic tracer deuterium, δD, and thus the deuterium excess $d = \delta D - 8\delta^{18}O$ [*Dansgaard*, 1964], used as a proxy of the climatic conditions (relative humidity, wind speed, and air temperature) at the evaporative (oceanic) moisture source [e.g., *Armengaud et al.*, 1998; *Hoffmann et al.*, 2001].

[6] The aim of this study is to compare the model results with the available observational IAEA-GNIP data to see how well the models reproduce the observed spatiotemporal distribution of $\delta^{18}O$ in precipitation. Given that the models perform reasonably well, we will then analyze what climatic controls act on $\delta^{18}O$ in precipitation under modern conditions over the tropical Americas (40°N–40°S/120°W–0°). In a companion paper [*Vuille et al.*, 2003], we use the same two models to simulate the stable isotopic composition of three ice cores from the tropical Andes.

[7] In the next section, we present the different model experiments and the observational data we used in this study. Section 3 includes a comparison of the diagnostics from the different model experiments with observational data from IAEA-GNIP and the National Centers for Environmental Prediction-National Center for Atmospheric Research (NCEP-NCAR) reanalysis project [*Kalnay et al.*, 1996]. Section 4 is a discussion of the relative importance of several climatic controls on stable isotope variability, such as temperature, precipitation amount, changes in moisture source, and the El Niño-Southern Oscillation (ENSO) phenomenon. Section 5 ends with a discussion of the results and some concluding remarks.

2. Model Experiments and Observational Database

[8] The AGCMs used in this study are the NASA-GISS II [*Hansen et al.*, 1983; *Jouzel et al.*, 1987] and the Hamburg ECHAM-4 isotope models [*Roeckner et al.*, 1996; *Hoffmann et al.*, 1998]. *Jouzel et al.* [1991] have demonstrated that the GISS model successfully reproduces the important features of present-day global isotope distributions, including the spatial correlations between isotope concentration and temperature at middle to high latitudes and between isotope concentration and precipitation amount at low latitudes. *Hoffmann et al.* [1998] have demonstrated the validity of the ECHAM model when simulating isotopic altitude effects in the Andes and the Himalayas, the amount effect in the tropics, and the effects of continentality and seasonality, and *Werner and Heimann* [2002] used the ECHAM-4 model to simulate interannual variability of $\delta^{18}O$ and δD in polar regions.

[9] Our GISS II experiments are based on a new version of the model, which includes a higher spatial resolution of 4°lat. × 5°long. with nine vertical layers based on sigma levels, running in improved double precision, and with improvements to the land surface radiation scheme, and replacement of the radiation module from model II′ [*Hansen et al.*, 1997]. The ECHAM-4 isotope model is based on a hybrid sigma-pressure coordinate system and was run with triangular truncation at both wave numbers 30 (T30 ∼ 3.75°lat. × 3.75°long.) and 106 (T106 ∼ 1.1°lat. × 1.1°long.) including 19 vertical layers from surface to 30 hPa.

Table 1. Setup of GISS II and ECHAM-4 Model Simulations

Model Simulation	Model Integration	Horizontal Resolution	Forcing	Topography	Tagging Capabilities
Control runs					
GISS II CTR-NORM	5 years	4° × 5°	global SST climatology	regular GISS II topography	Yes
GISS II CTR-RAIS	5 years	4° × 5°	global SST climatology	Andean Cordillera raised to 90th percentile	Yes
ECHAM-4 T30 CTR	10 years	~3.75° × 3.75°	global SST climatology	regular T30 topography	Yes
Modern climate simulations					
GISS II	1980–97	4° × 5°	observed global SST 1980–97	Andean Cordillera raised to 90th percentile	Yes
ECHAM-4 T30	1950–94	~3.75° × 3.75°	observed global SST, greenhouse gases 1950–94	regular T30 topography	No
ECHAM-4 T106	1979–98	~1.1° × 1.1°	observed global SST 1979–98	regular T106 topography	No

[10] All three model experiments (GISS II, ECHAM-4 T30, ECHAM-4 T106) were run with modern boundary conditions and forced with observed global sea surface temperatures (SST). The GISS simulation is based on atmospheric model intercomparison project I (AMIP I) and Reynolds Optimum Interpolation SST, while the ECHAM model uses global sea-ice and sea surface temperature 2.2 (GISST 2.2) data. While greenhouse gas concentrations were kept at a constant modern level in the GISS II and the ECHAM-4 T106 runs, these levels were adjusted annually in the ECHAM-4 T30 experiment (Table 1). The three experiments were run for an unequal length of time, which should be kept in mind when comparing output between the different simulations. ECHAM-4 T30 is the longest run, starting in 1903, but we limit our analysis to the period 1950–1994, for which the SST forcing is more reliable and the model performance can realistically be evaluated using NCEP-NCAR reanalysis and IAEA-GNIP stable isotope data. The ECHAM-4 T106 (1979–1998) and the GISS II (1980–1997) experiments essentially cover the last two decades. The first year in all the runs was discarded to avoid data problems with model equilibration during spin-up time.

[11] The GISS II model further includes isotopic tracers, that is, water evaporating from a source is tagged upon evaporation and the tag is only lost when the water molecule falls as precipitation. Thus water molecules precipitating over the targeted areas can be traced back to their evaporative source area [*Koster et al.*, 1986]. This allows us to quantify exactly the relative contribution of different evaporative source regions to a region's given precipitation and to assess the $\delta^{18}O$ signature of the different source regions over each grid cell [*Charles et al.*, 1994]. We divided the global grid into 26 continental and oceanographic regions, each of which encompasses a zone with a reasonably uniform climate (Figure 1a). The model tracks both changes in the isotopic content of precipitation and the contribution to local precipitation from each of these 26 regions. Since we limit the analysis of our results to the tropical Americas, only a subsample of the 26 source regions will be shown and discussed. A similar tagging experiment was performed in a 10-year control simulation with the ECHAM-4 model in T30 resolution, using modern SST climatology. The source region delineation (Figure 1b) is based on the mean SST field [*Werner et al.*, 2001] and therefore somewhat different from the GISS experiment, where the applied source region delineation is strictly zonal.

[12] Both the GISS II and the ECHAM-4 T106 model experiments have an improved horizontal resolution, when compared to earlier studies [e.g., *Cole et al.*, 1993, 1999; *Hoffmann et al.*, 1998]. While the topography in the ECHAM T106 model resolves the Andean cordillera in a reasonable manner, the 4°lat. × 5°long. resolution of the GISS model is still too coarse for an accurate representation of the Andes. In order to better reflect this topographical

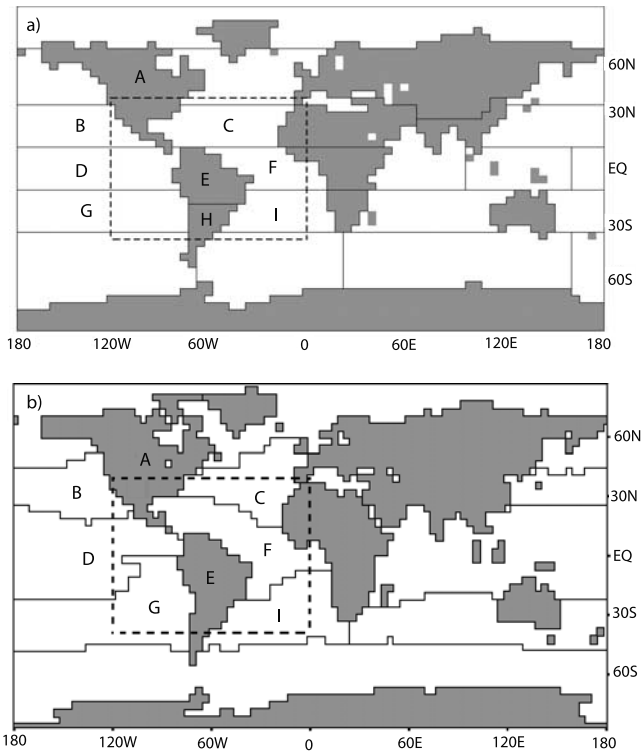

Figure 1. Source regions for tagging experiments of water vapor and $\delta^{18}O$ of precipitation in (a) GISS II (1980–1997) and (b) ECHAM-4 T30 CTR simulation [*Werner et al.*, 2001]. Source regions relevant to the tropical Americas regions (outlined in dashed thick black line) are indicated with capital letters: A, North America; B, tropical North Pacific; C, tropical North Atlantic; D, equatorial Pacific; E, tropical South America; F, equatorial Atlantic; G, tropical South Pacific; H, subtropical South America; and I, tropical South Atlantic. Note that H forms part of region E in Figure 1b.

wall in the atmosphere created by the Andes, we therefore changed the grid cell elevation in the GISS model along the Andes from the 50th percentile (z_{50}) to the 90th percentile (z_{90}). The new grid cell elevation z_{90} was determined by means of a 30′ digital elevation model (GTOPO 30) and is defined as the elevation at which 90% (10%) of the area within each 4° × 5° grid cell lies below (above) z_{90}. This procedure resulted in Andean cordillera grid cells reaching elevations as high as 4500 m in the Central Andes, while before the highest grid cell did not exceed 2580 m. Since such a procedure may cause severe changes in the modeled atmospheric circulation, we performed a 7-year control run with both the conventional (GISS CTR-NORM) and the new raised topography (GISS CTR-RAIS) to investigate the effects of the raised topography before applying it to the GISS 1980–1997 experiment. The first two simulation years were used for model spin-up and excluded from the analysis of the control experiments. No changes in topography were applied to the ECHAM simulations. An overview over the different model experiments is given in Table 1.

[13] The model performance is analyzed in section 3 based on NCEP-NCAR reanalysis fields [*Kalnay et al.*, 1996] and the IAEA-GNIP stable isotope database. The NCEP-NCAR reanalysis fields are not purely observational, but represent a blend between observational and model data. Nonetheless, they are considered to quite realistically portray the state of the atmosphere on diurnal to interannual timescales. We used monthly data of surface temperature and precipitation on a 2.5° × 2.5° grid between 1950 and 1998. In addition, we extracted monthly data of surface temperature, precipitation, and $\delta^{18}O$ in precipitation from all available IAEA-GNIP stations between 40°N and 40°S and 120°W and 0° with a record length of at least 24 months.

3. Model Performance

3.1. Mean Climate

[14] The long-term mean precipitation (Figure 2) and surface air temperature (Figure 3) patterns during austral (DJF) and boreal summer (JJA) for both GISS II control runs and all modern climate simulations are shown and compared with the observational output from NCEP-NCAR reanalysis. All experiments capture the essential characteristics of summer precipitation over the tropical Americas (Figure 2), that is, the seasonal shift of the intertropical convergence zone (ITCZ) over the tropical oceans and the change in the location of the respective summer season maximum over the tropical continent. The ECHAM-4 T30 experiment (Figures 2c and 2d) shows the strongest resemblance to the NCEP-NCAR data in both DJF and JJA (Figures 2a and 2b), but it also represents a long-term mean averaged over an almost identical time period. The precipitation is nonetheless somewhat underestimated over northern tropical South America in JJA in both ECHAM simulations. The ECHAM-4 T106 experiment overestimates precipitation along the ITCZ over the tropical Oceans, especially in JJA and features a too strong meridional precipitation gradient toward the north and south of the ITCZ (Figures 2e and 2f). GISS CTR-NORM and to a lesser degree GISS CTR-RAIS also overestimate precipitation along the ITCZ in DJF, but both models underestimate the precipitation maximum over Central America in JJA. Because of their coarser resolution, they are also unable to resolve some of the mesoscale features associated with summer precipitation. When comparing the simulated precipitation fields with the NCEP-NCAR data, it should be kept in mind that NCEP-NCAR precipitation, although capturing the broad climatological patterns, is itself somewhat biased over tropical South America. *Costa and Foley* [1998], for example, have shown that artificial undulations occur next to the Andes, such as the wet/dry/wet pattern seen in Figure 2a near the Central Andes, and *Liebmann et al.* [1998] concluded that the amplitude of the annual cycle over tropical South America is too small in the NCEP-NCAR data.

[15] The surface temperature field in Figure 3 is also well reproduced by all models. The major deficiency is associated with the high topography, which is not resolved well enough in the ECHAM-4 T30 (Figures 3c and 3d) and the GISS CTR-NORM (Figures 3g and 3h) experiments. This leads to temperatures that are too high when compared to the NCEP-NCAR data (Figures 3a and 3b). The GISS CTR-RAIS experiment (Figures 3i and 3j) and the high-resolution simulation ECHAM-4 T106 (Figures 3e and 3f), however, are able to reproduce the colder temperatures at high elevations in the Andes, although the cold wedge is too broad due to the coarser resolution in the GISS CTR-RAIS experiment. The ECHAM-4 T106 experiment, on the other hand, features higher temperatures than the NCEP-NCAR fields or any of the other models. This may be partially caused by the more recent time period (1979–1998) with higher average SST over which the T106 experiment was integrated. Finally, differences between the models and NCEP-NCAR reanalysis data over oceanic regions may also reflect the use of different SST data sets.

3.2. Spatial Distribution of $\delta^{18}O$ in Precipitation

[16] The annual mean composition of $\delta^{18}O$ in precipitation is reproduced in a satisfactory way by all model experiments (Figure 4). Since precipitation in the tropics and subtropics shows a strong seasonality, a simple average based on the monthly $\delta^{18}O$ data would be heavily biased toward the drier months. All fields in Figure 4 have therefore been weighted by the amount of precipitation in each month before averaging. The heaviest values occur over the oceans, especially in the dry regions of the subtropical anticyclones. The most depleted values over the oceans are associated with the ITCZ, which leaves a distinct imprint of more negative values near the equator. A stronger

Figure 2. (opposite) Long-term average precipitation (in mm/day) for DJF (left column) and JJA (right column). (a–b) NCEP-NCAR reanalysis (1961–1990), (c–d) ECHAM-4 T30 (1961–1990), (e–f) ECHAM-4 T106 (1979–1998), (g–h) GISS II CTR-NORM, and (i–j) GISS II CTR-RAIS. Contour intervals are 2, 4, 8, and 12 mm/day, and values >4 (8) mm/day are shaded in light (dark) gray.

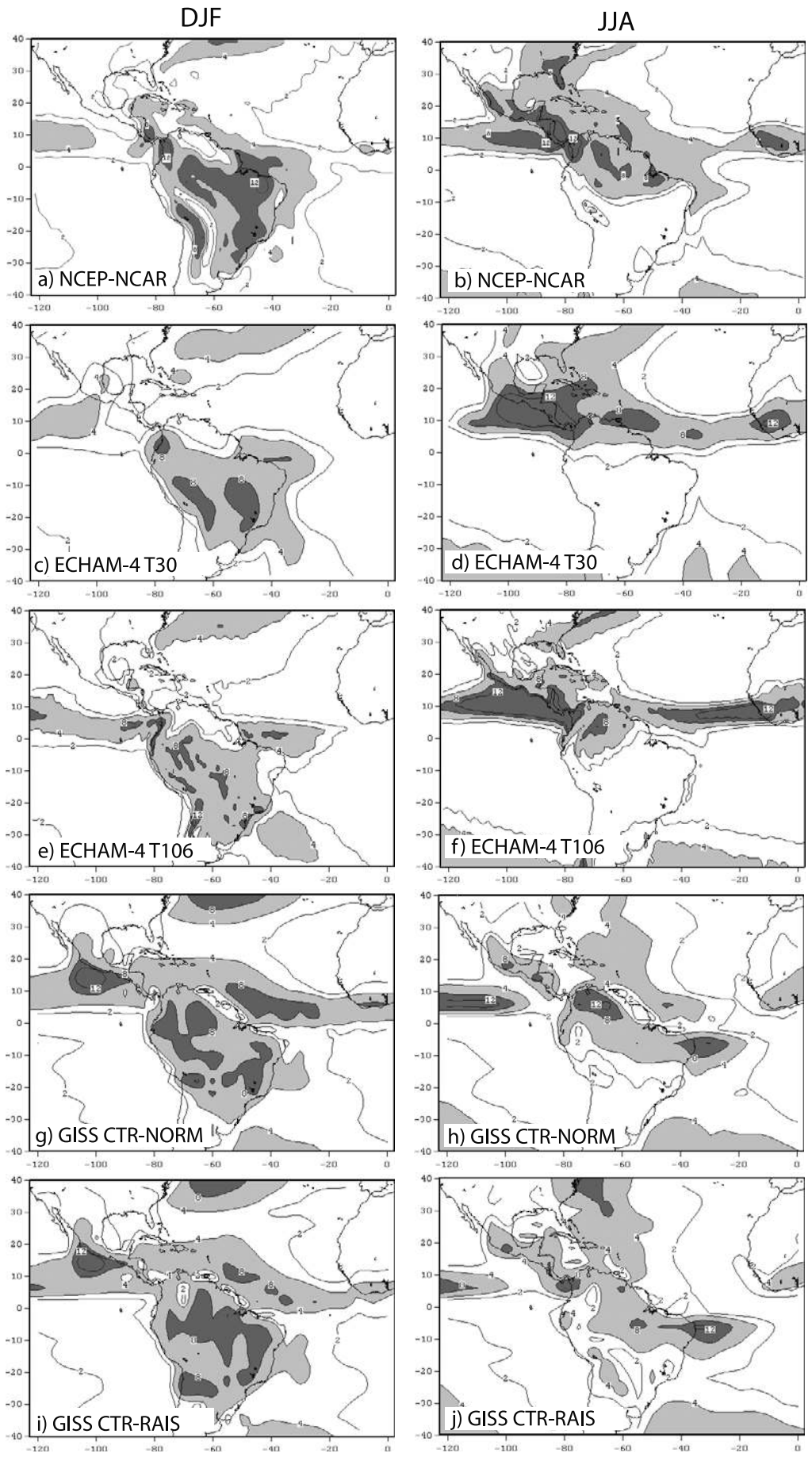
DJF
JJA
a) NCEP-NCAR
b) NCEP-NCAR
c) ECHAM-4 T30
d) ECHAM-4 T30
e) ECHAM-4 T106
f) ECHAM-4 T106
g) GISS CTR-NORM
h) GISS CTR-NORM
i) GISS CTR-RAIS
j) GISS CTR-RAIS

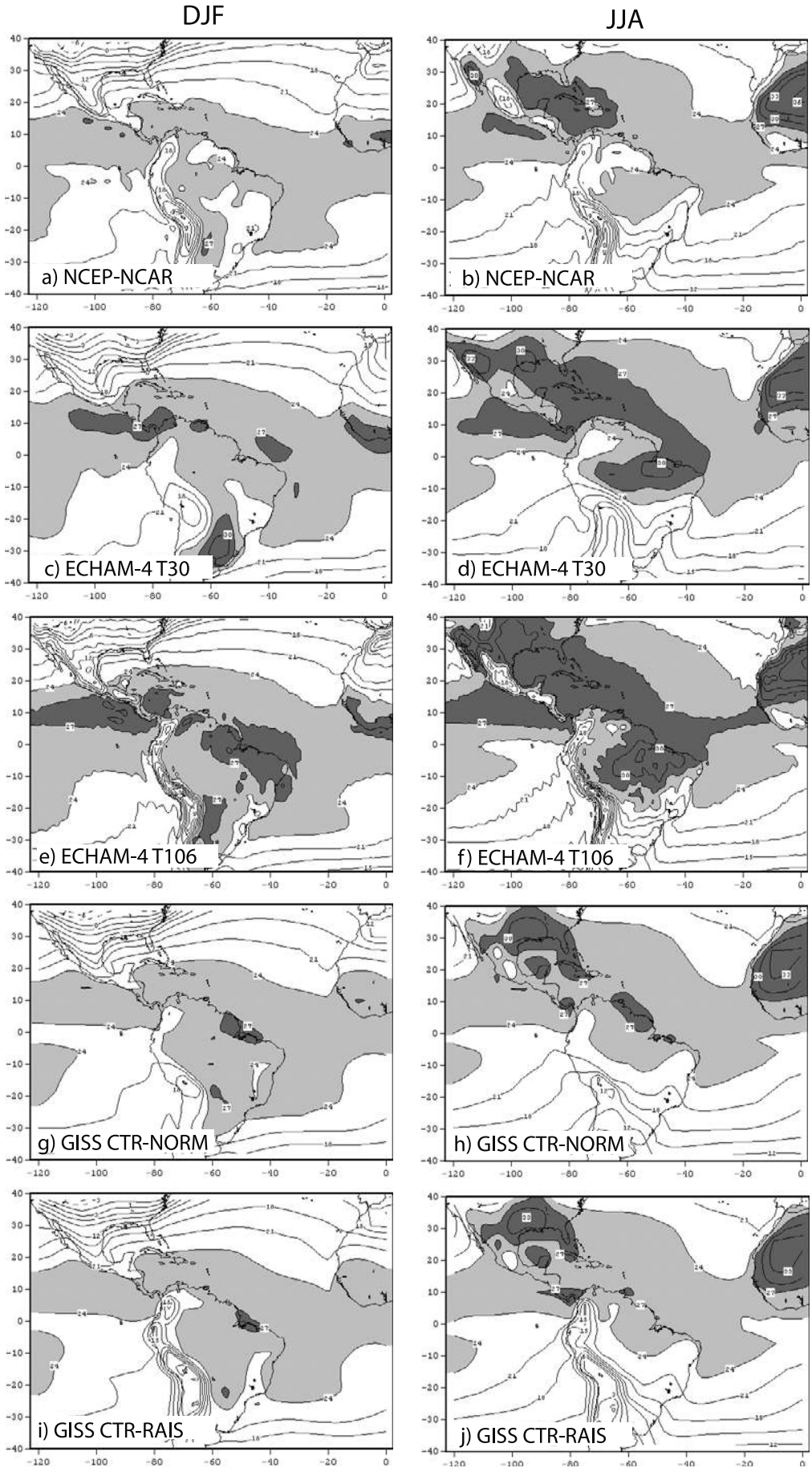
DJF
JJA
a) NCEP-NCAR
b) NCEP-NCAR
c) ECHAM-4 T30
d) ECHAM-4 T30
e) ECHAM-4 T106
f) ECHAM-4 T106
g) GISS CTR-NORM
h) GISS CTR-NORM
i) GISS CTR-RAIS
j) GISS CTR-RAIS

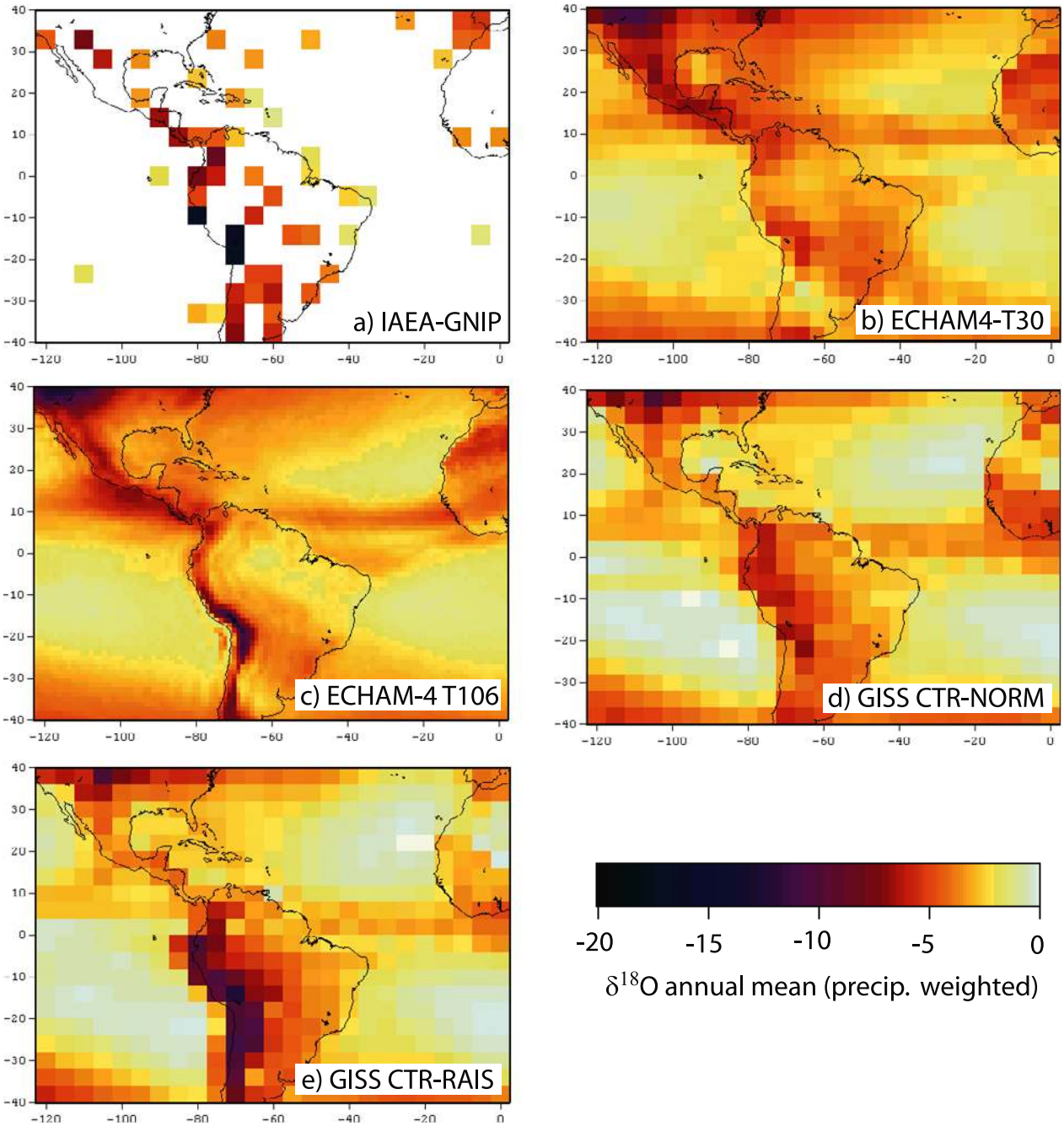

Figure 4. Annual mean $\delta^{18}O$ of precipitation in (a) IAEA station data (varying record lengths) and modern ice core records from Quelccaya, Huascarán, and Sajama [*Thompson et al.*, 1985, 1995, 1998], (b) ECHAM-4 T30 (1950–1994), (c) ECHAM-4 T106 (1979–1998), (d) GISS II CTR-NORM, and (e) GISS II CTR-RAIS. The annual mean of $\delta^{18}O$ is weighted by the monthly mean precipitation amount.

depletion occurs near the northern and southern edges of the study area toward the midlatitudes. This is especially apparent over the continental US. Finally, the effects of continentality and altitude are apparent in the observational data. That is, regions further inland and at higher elevations show increasingly depleted values; these are features which are reproduced by the models to some extent and discussed in more detail in section 3.4. The correlation coefficients between annual mean precipitation-weighted $\delta^{18}O$ of the 62 IAEA stations and the corresponding grid cell values from the model simulations are as follows: GISS-CTR-NORM, 0.79; GISS-CTR-RAIS, 0.79; ECHAM-4-T30, 0.44; and

Figure 3. (opposite) As in Figure 2, but for surface air temperature (2 m above ground, in °C). Contour intervals are 3°C, and values >24°C (27°C) are shaded in light (dark) gray.

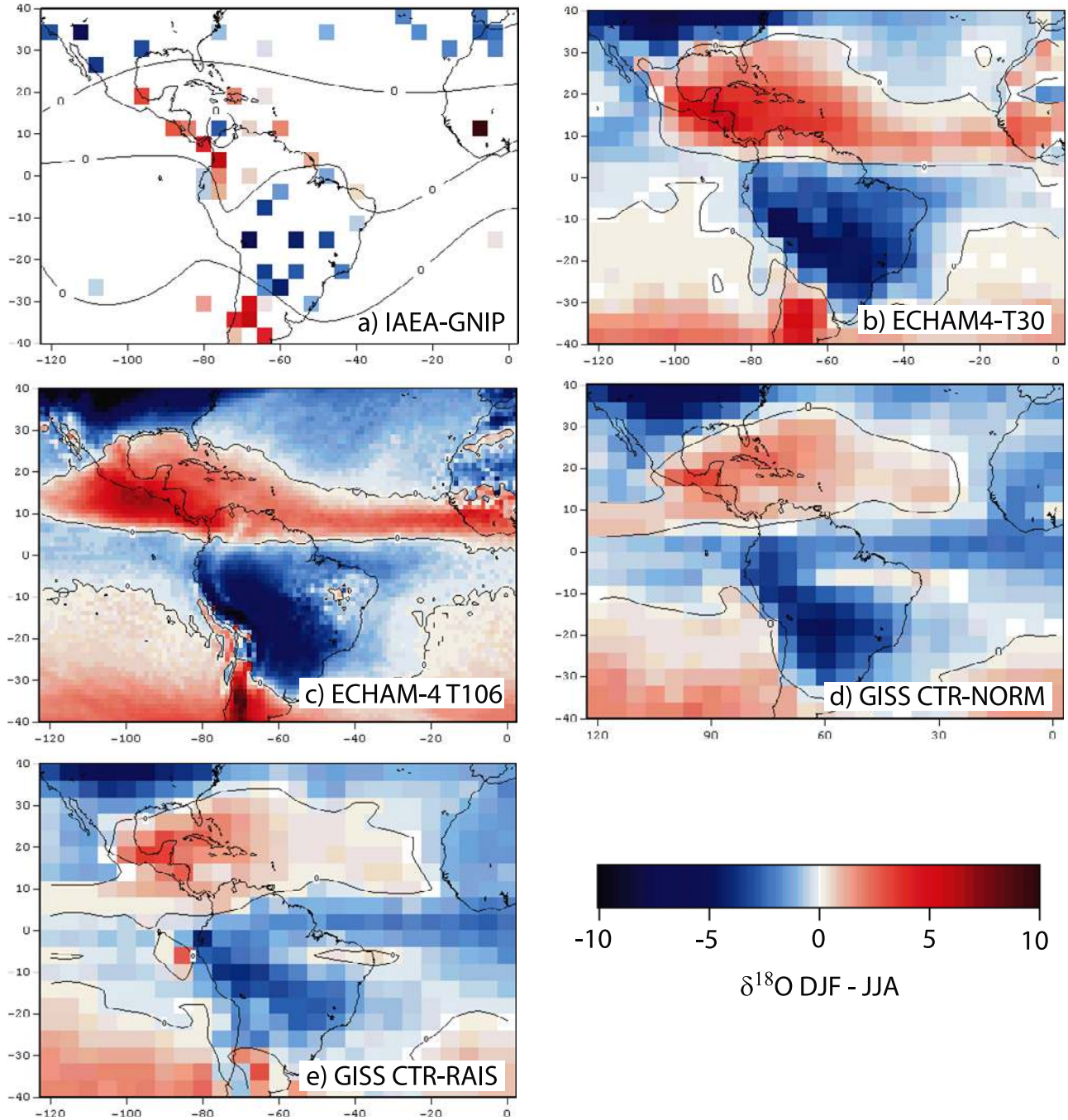

Figure 5. DJF-JJA $\delta^{18}O$ of precipitation for (a) IAEA station data, (b) ECHAM-4 T30, (c) ECHAM-4 T106, (d) GISS II CTR-NORM, and (e) GISS II CTR-RAIS.

ECHAM-4-T106, 0.69. It should be kept in mind that these correlations compare simulated data with varying periods of model integration (Table 1) and IAEA data, which are often based on very short periods of observation. The magnitudes of the resulting correlation coefficients are, therefore, not directly comparable between the various models.

3.3. Seasonality of Precipitation

[17] Figure 5 shows the difference between the weighted mean $\delta^{18}O$ values for austral (DJF) and boreal summer (JJA) illustrating the ability of the models to accurately portray the modern seasonality of precipitation. Four distinct latitudinal zones can be identified in the observational data (Figure 5a) with a coherent signal of positive or negative values. In the midlatitudes of the northern (southern) hemisphere, the $\delta^{18}O$ difference DJF-JJA is negative (positive) because temperature represents the dominant controlling factor on the seasonal timescale and values are more depleted during the winter season, DJF (JJA). Toward lower latitudes, however, the signal shows a distinct reversal in both hemispheres with more depleted values during the respective summer season. Here on the seasonal timescale, the $\delta^{18}O$ value is clearly controlled by the precipitation

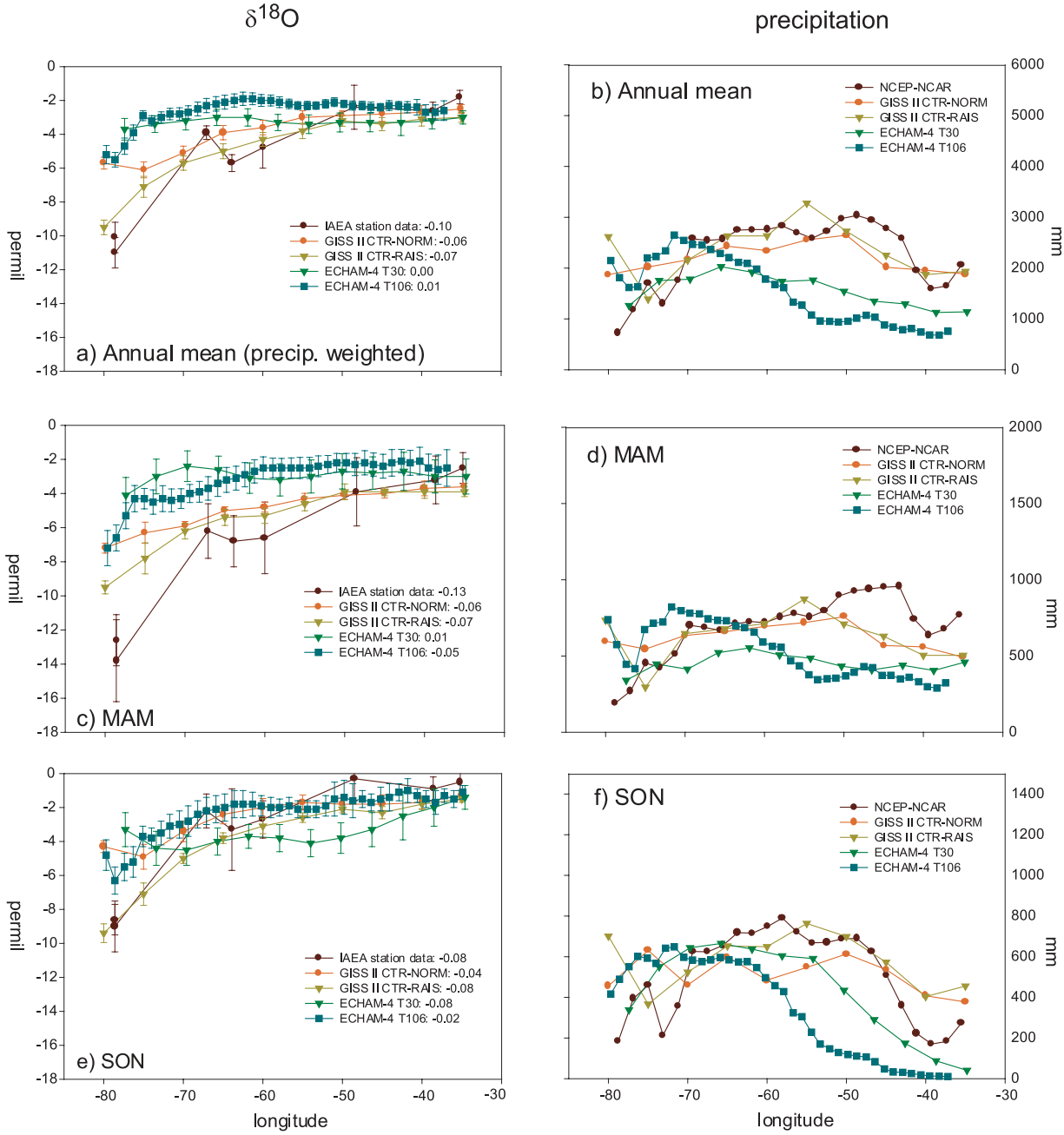

Figure 6. Continental gradient of $\delta^{18}O$ of precipitation and precipitation amount across the Amazon basin from Atlantic coast at 35°W to the Andean crest at 80°W. (a) Annual mean $\delta^{18}O$ (in permil, weighted by precipitation), (b) annual mean precipitation (mm), (c) as in Figure 6a but for MAM, (d) as in Figure 6b but for MAM, (e) as in Figure 6a but for SON, and (f) as in figure 6b but for SON. Model and NCEP-NCAR data are latitudinal average between approximately 0° and 10°S (depending on grid size) including grid cells over land only; station data shows IAEA observations between 0° and 10°S. Error bars extend to one standard deviation on either side of long-term mean. Numbers in legend refer to continental slope, that is the change in $\delta^{18}O$ per unit longitude (in ‰/°) between 35° and 70°W.

amount and therefore more depleted values occur during the rainy season, that is, in JJA (DJF) to the north (south) of the equator. The change from precipitation to temperature controlled $\delta^{18}O$ value is thus marked by the northward limit of tropical summer precipitation in both hemispheres [*Araguás-Araguás et al.*, 1998]. Annually resolved $\delta^{18}O$ paleo-records along this boundary might offer the potential to reconstruct paleomonsoon intensity and the past extent of the ITCZ. Both the ECHAM-4 model (Figures 5b and 5c) and the GISS II control experiments (Figures 5d and 5e) simulate the spatial extent of the different zones as indicated by the IAEA station data (Figure 5a). The only notable

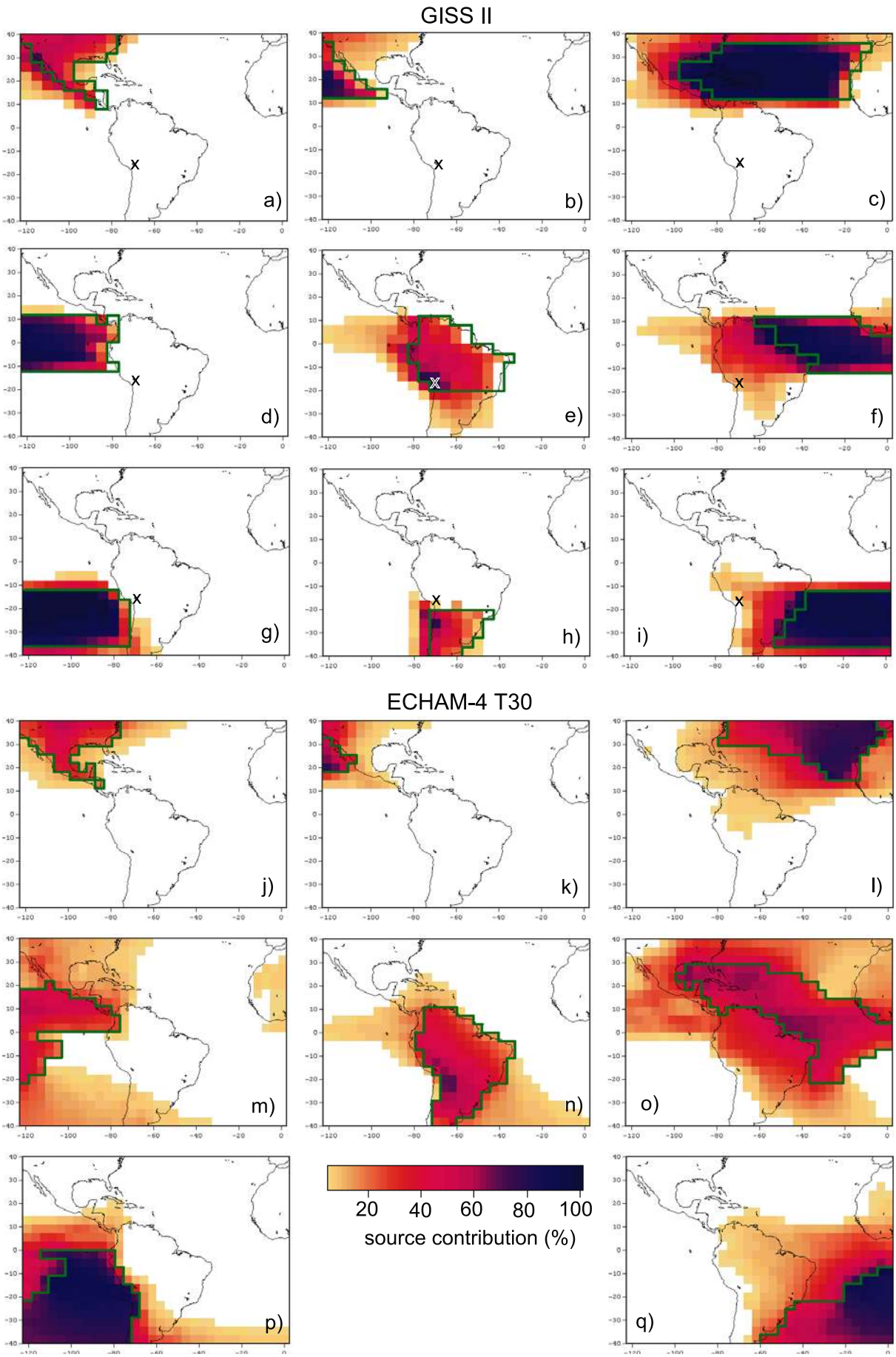
GISS II
a)
b)
c)
d)
e)
f)
g)
h)
i)
ECHAM-4 T30
j)
k)
l)
m)
n)
o)
p)
q)
20 40 60 80 100
source contribution (%)

exception occurs over the West African summer monsoon region, where the more depleted values in JJA are not apparent in the GISS II simulations.

3.4. Continentality and Altitude Effect

[18] The effect of continentality and altitude on the $\delta^{18}O$ composition of precipitation is investigated along a transect through tropical South America, following the major trajectory of moisture from the Atlantic coast near 35°W across the Amazon basin toward the tropical Andean ridge near 80°W (Figure 6). Rather than showing the continentality effect for austral and boreal summers, we chose the main rainy (MAM) and dry seasons (SON) over the Amazon basin to discuss the effects of water vapor transport, rainout, and evapotranspiration on the $\delta^{18}O$ composition of precipitation. During the rainy season (MAM), the values are more depleted than during the dry season (SON), but the general isotopic depletion as air masses move inland clearly occurs in both seasons, thus contradicting the assumption of no dry season depletion, made in earlier attempts to interpret the stable isotopic record of tropical Andean ice cores [*Grootes et al.*, 1989].

[19] Not all model experiments are able to capture the essential features of both the effects of continentality and altitude in a similar way. While the GISS control runs show a depletion of ~0.07‰/° longitude, which is quite similar to observations (~0.1‰/° longitude); the inland depletion is too weak in the ECHAM-4 models during MAM and realistically simulated only during the dry season. As a result, ECHAM-4 T30 has $\delta^{18}O$ values over the tropical Andes near 80°, which are too enriched. There are several reasons that may account for this deficit, but most importantly, the precipitation amount is underestimated in both ECHAM simulations over the eastern Amazon basin (Figures 6b, 6d, and 6f). This deficit in simulated rainout along the trajectory of air masses moving inland results in more enriched $\delta^{18}O$ values.

[20] The altitude effect between 70° and 80°W, however, is correctly simulated in the higher-resolution version of the ECHAM-4 model (T106), which thus also produces more realistic $\delta^{18}O$ values over the tropical Andes. While both GISS control runs nicely simulate the continentality effect, GISS-CTR-NORM shows essentially no altitude effect due to the poor representation of the Andean topography. GISS-CTR-RAIS, however, simulates $\delta^{18}O$ values that are much more depleted and quite similar to the observed data over the tropical Andes, particularly for the annual mean and the dry season.

3.5. Moisture Source Contributions

[21] Figure 7 shows the annual mean contribution (in percent) of source regions to precipitation in each grid cell over the tropical Americas for the GISS II 1980–1997 simulation and the ECHAM-4 T30 CTR run. Each plot shows the contribution of one source region, outlined in green for clarity, to modeled precipitation over all grid cells. The source regions are the same as shown in Figure 1. The contribution from each source is only shown over grid cells where it contributes at least 5% to the annual mean precipitation. For example, the Central Andes (marked with a "cross" in Figures 7a–7i) receive precipitation from only four different moisture source areas: ~70% from tropical South America (Figure 7e), ~15% from the tropical North Atlantic (Figure 7f), ~5% from subtropical South America (Figure 7h) and ~10% from the tropical South Atlantic (Figure 7i). Generally, the contribution of a local source is higher over the oceans, while land areas, such as the southern United States or tropical and subtropical South America, experience a high contribution of moisture influx from the tropical Atlantic, and in the case of the US, also from the subtropical North Pacific. Their precipitation is thus a mix of continental, reevaporated moisture, and long-range transport from an oceanic source. The modeled vapor transport is similar between the two models, given the differences in the source region delineations between the two experiments. The most apparent differences are related to the long-range water vapor transport, which seems much more restricted in the GISS simulation. Nonetheless, the results from both simulations are largely consistent with evidence from observational studies indicating significant moisture influx from the tropical Atlantic into the South American continent [e.g., *Victoria et al.*, 1991; *Eltahir and Bras*, 1994; *Rao et al.*, 1996; *Vuille et al.*, 1998; *Costa and Foley*, 1999; *Curtis and Hastenrath*, 1999], while the low-level inversion over the eastern Pacific and the blocking effect of the Andes allows no moisture to penetrate eastward into the continent [*Garreaud et al.*, 2003].

[22] A comparison of the two GISS II control experiments (not shown) further indicates that the raised topography leads to a more realistic separation of precipitation evaporating from sources to the east and the west of the Andes. The contribution of moisture evaporating over tropical South America to precipitation over the Pacific, for example, is largely reduced, and a higher fraction is transported poleward instead, contributing to local precipitation over the subtropical continent, consistent with observations [e.g., *Berri and Inzunza*, 1993; *Nogués-Paegele and Mo*, 1997]. The variability on interannual timescales is rather low, that is the percent contribution from the different moisture sources to a given grid cell's precipitation remains fairly constant over time, which may reflect the limited long-range water vapor transport simulated in the GISS model. Even during El Niño and La Niña years, when the absolute precipitation amounts can undergo large fluc-

Figure 7. (opposite) Annual mean contribution (in percent) of source regions to precipitation in each grid cell. (a–i) GISS II model (1980–1997) and (j–q) ECHAM-4 T30 CTR simulation. Note that source regions, outlined in green for clarity, are somewhat different between the two models (see Figure 1). (Figures 7a and 7j) North America (source region A); (Figures 7b and 7k) tropical North Pacific (B); (Figures 7c and 7l) tropical North Atlantic (C); (Figures 7d and 7m) equatorial Pacific (D); (Figures 7e and 7n) tropical South America (E); (Figures 7f and 7o) equatorial Atlantic (F); (Figures 7g and 7p) tropical South Pacific (G), (Figure 7h) subtropical South America (H); and (Figures 7i and 7q) tropical South Atlantic (I). Results are only shown where the respective source region contributes >5% to annual precipitation total. "Cross" denotes location of the Central Andes (see text for detailed interpretation).

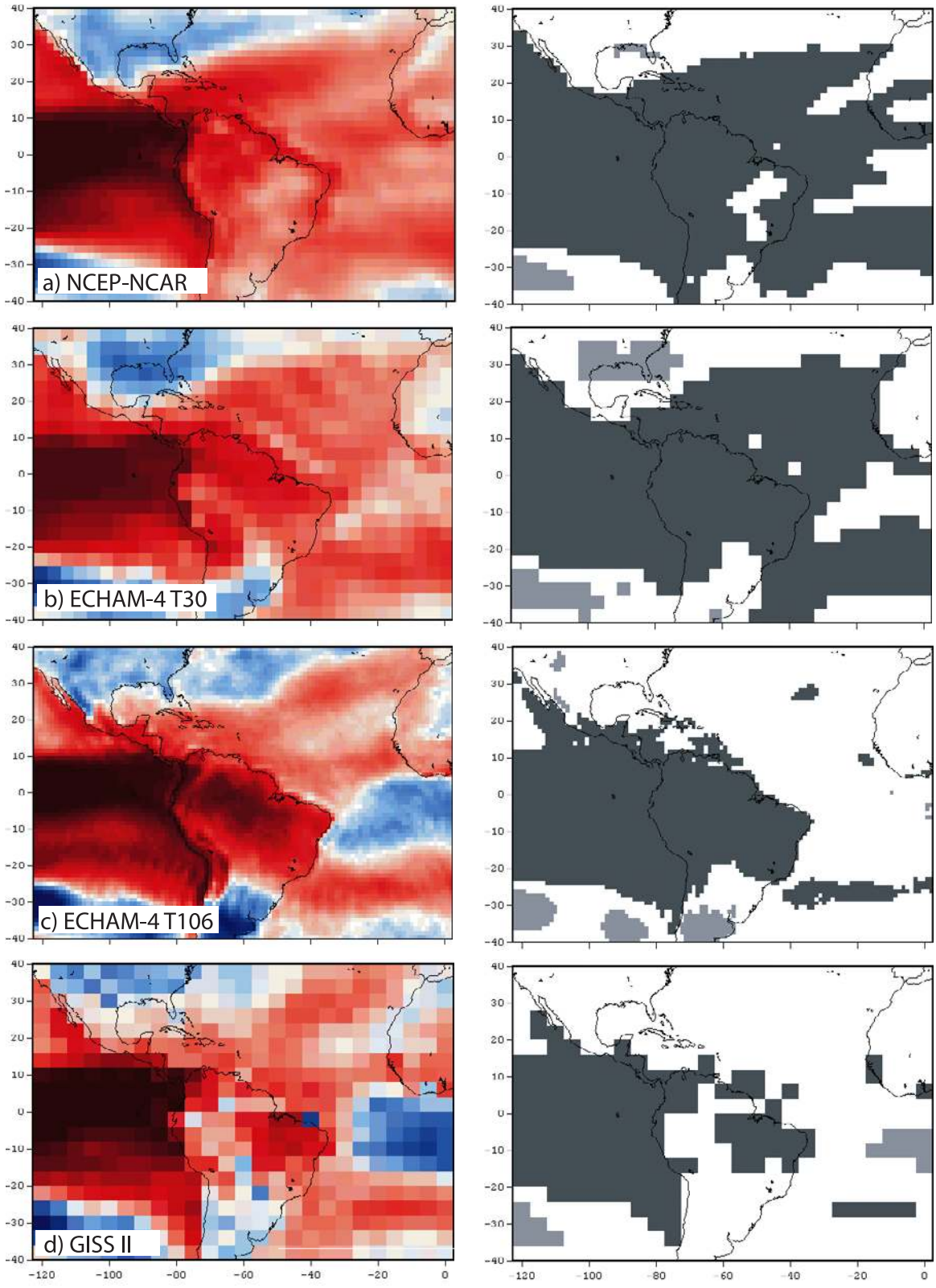
a) NCEP-NCAR
b) ECHAM-4 T30
c) ECHAM-4 T106
d) GISS II
-120 -100 -80 -60 -40 -20 0
-0.8 -0.4 0 0.4 0.8
Corr.coeff. (r) Niño3.4 vs. temperature

tuations in certain regions, the relative contributions from the various sources remain quite similar [see *Vuille et al.*, 2003].

3.6. Interannual Variability (ENSO)

[23] A further aspect of evaluating model performances is to assess their capability to simulate interannual climate changes. ENSO is the strongest climatic signal on interannual timescales and has a significant imprint on climate in many parts of the tropical Americas [e.g., *Bradley et al.*, 1987; *Aceituno*, 1988, 1989; *Kiladis and Diaz*, 1989; *Halpert and Ropelewski*, 1992; *Ropelewski and Halpert*, 1996]. In order to analyze how realistically the simulations portray the ENSO relationship with different climate variables over the tropical Americas, we compared the correlation field between the NINO3.4 index (sea surface temperature anomalies (SSTA) averaged over 5°N–5°S; 120°W–170°W) and both simulated and observed surface climates. Figure 8 shows the NINO3.4 correlation with monthly surface temperature anomalies in the NCEP-NCAR reanalysis data and model simulations. The right column shows regions with a significant positive (negative) correlation at the 95% confidence level, based on a two-tailed Student's *t*-test, shaded in dark (light) gray. All models reproduce the well-known warming (cooling) of the tropics associated with the ENSO warm (cold) phase. The inverse relationship between ENSO and temperature response in the midlatitudes of both hemispheres is identically captured by all three experiments, although it seems to be overestimated by the simulations over southern South America. The only major discrepancy occurs over the tropical South Atlantic where the two shorter simulations GISS II and ECHAM-4 T106 produce a negative correlation between surface temperature and the NINO3.4 index. However, if the correlation is calculated for the same short time period in the reanalysis data, it is apparent there as well (not shown). This discrepancy is thus most likely produced by a change in the ENSO influence over this region during the last 20 years. The lack of significant correlations over the tropical Atlantic in the GISS II and ECHAM-4 T106 simulations results from the short period of integration and thus the reduced degrees of freedom, but the GISS II experiment also fails to reproduce a significant correlation over parts of tropical South America.

[24] A composite analysis is used to analyze the ENSO influence on precipitation. The first (third) row in Figure 9 represents the precipitation difference (in percent) between El Niño and La Niña periods during DJF (JJA), with precipitation during El Niño considered as 100%. The row below shows the regions, which feature a significant precipitation difference between these two extreme phases of ENSO, shaded in gray. El Niño (La Niña) phases used in this composite analysis are based on a definition similar to the one by *Trenberth* [1997], but we used a slightly higher threshold (0.5°C instead of 0.4°C) and a slightly different reference period (1951–1980 instead of 1950–1979) to compute the monthly anomalies. An El Niño (La Niña) event thus occurred if the 5-month running mean of SSTA in the NINO3.4 region exceeds (or remains below) 0.5°C (−0.5°C) for at least 6 consecutive months. The ENSO periods based on this definition are listed in Table 2.

[25] The major ENSO-related precipitation anomalies over the tropical Americas are captured by the NCEP-NCAR reanalysis composites in DJF (Figure 9a) and JJA (Figure 9e). In DJF, these anomalies include an El Niño-induced precipitation deficit over the southern Carribean [e.g., *Giannini et al.*, 2000], northern tropical South America [e.g., *Aceituno*, 1988; *Rogers*, 1988; *Hastenrath*, 1990; *Poveda and Mesa*, 1997], and the tropical Andes [*Vuille*, 1999; *Vuille et al.*, 2000a, 2000b; *Garreaud and Aceituno*, 2001; *Garreaud et al.*, 2003] and a precipitation surplus over the eastern equatorial Pacific and the west coast of South America [e.g., *Horel and Cornejo-Garrido*, 1986; *Goldberg et al.*, 1987; *Deser and Wallace*, 1990; *Tapley and Waylen*, 1990; *Bendix*, 2000] and the southern United States [e.g., *Montroy*, 1997]. All simulations reproduce the El Niño-related precipitation increase over the eastern equatorial Pacific and the decrease over northern tropical South America extending into the tropical North Atlantic, consistent with results from previous studies [e.g., *Moron et al.*, 1998]. There are, however, also significant differences between the three experiments. The ECHAM-4 T30 simulation underestimates the precipitation increase over the equatorial Pacific and produces a negative precipitation difference near the coast of South America (Figure 9b). The ECHAM-4 T30 and the GISS II simulations both fail to reproduce the wet conditions associated with El Niño over the southern United States. The T106 simulation on the other hand, due to the steep meridional precipitation gradient across the equator described in section 3.1, underestimates the latitudinal extent of the ENSO-related precipitation anomaly over the equatorial Pacific (Figure 9c).

[26] In JJA the ENSO-signal is usually less prominent in the tropics but instead shows a strong teleconnection pattern to the southern hemisphere midlatitudes [e.g., *Mo and Higgins*, 1998; *Garreaud and Battisti*, 1999]. Indeed, the NCEP-NCAR reanalysis field features a significant precipitation surplus during El Niño (as compared to La Niña) over the midlatitudes of South America (Figure 9e). This is consistent with evidence from Chile and Argentina [e.g., *Rutllant and Fuenzalida*, 1991; *Montecinos et al.*, 2000], Uruguay [e.g., *Pisciottano et al.*, 1994; *Diaz et al.*, 1998], and southern Brazil [*Grimm et al.*, 1998, 2000]. The ECHAM simulations quite accurately portray the southern hemisphere midlatitude precipitation field associated with ENSO (Figures 9f and 9g), but the GISS experiment erroneously produces a precipitation decrease during El Niño as compared to La Niña years (Figure 9h). The precipitation surplus in SE Brazil during El Niño years is apparent in the ECHAM models, but the deficit to the north over NE Brazil is too strong and displaced anomalously far to the south, and the T106 simulation underestimates the

Figure 8. (opposite) Correlation between NINO3.4 SSTA and monthly surface temperature anomalies. Left column shows correlation pattern, right column shows regions with significant positive (negative) correlation at the 95% confidence level in dark (light) gray shading. (a) NCEP-NCAR reanalysis (1950–1998), (b) ECHAM-4 T30 (1950–1994), (c) ECHAM-4 T106 (1979–1998), and (d) GISS II (1980–1997).

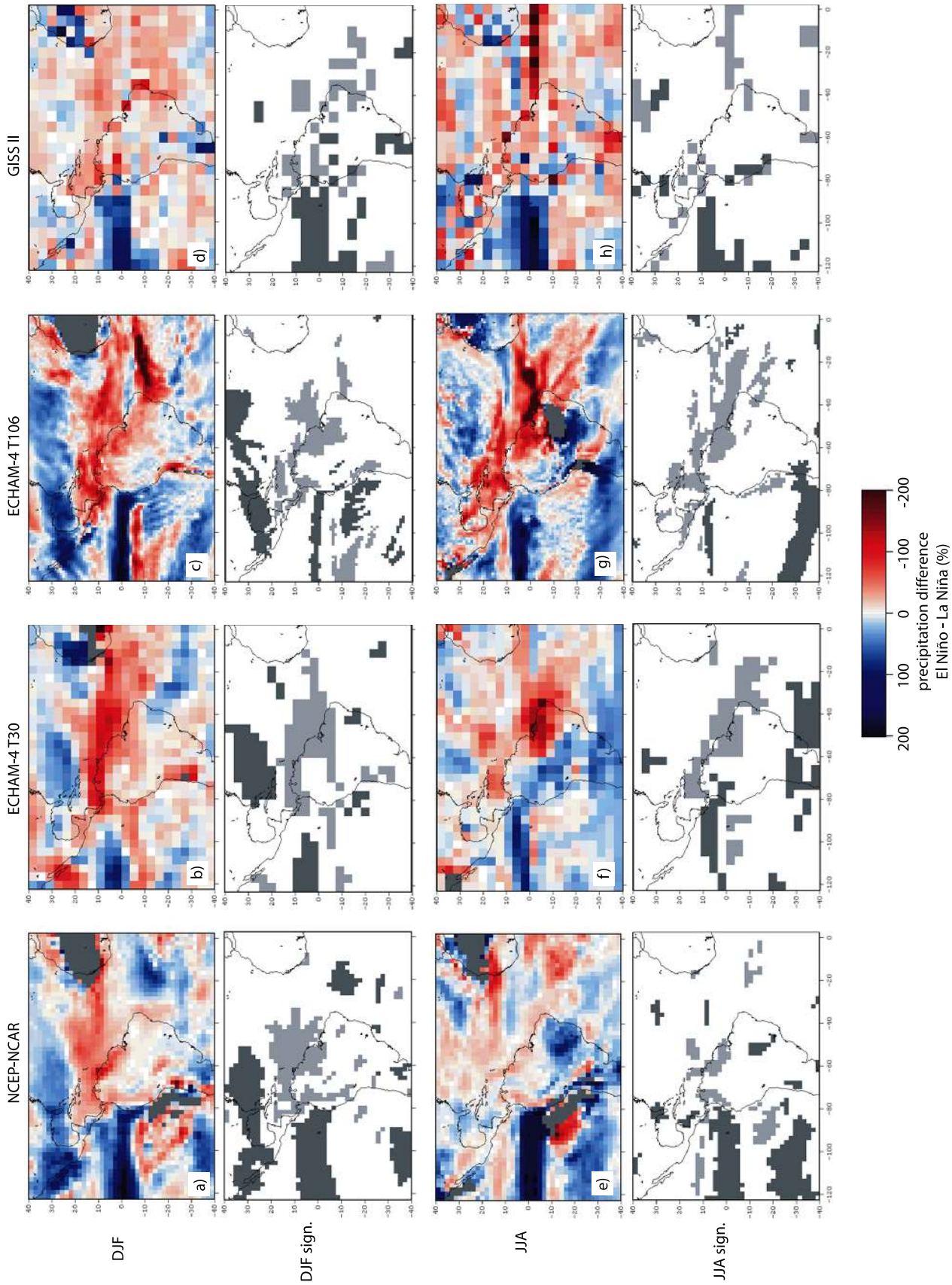
NCEP-NCAR
ECHAM-4 T30
ECHAM-4 T106
GISS II
DJF
DJF sign.
JJA
JJA sign.
a)
b)
c)
d)
e)
f)
g)
h)
200
100
0
-100
-200
precipitation difference
El Niño - La Niña (%)

Table 2. El Niño and La Niña Periods Between 1951 and 1998[a]

El Niño Events	La Niña Events
May 1957 to June 1958	July 1954 to March 1956
July 1963 to January 1964	May 1964 to January 1965
May 1965 to May 1966	July 1970 to January 1972
October 1968 to February 1970	June 1973 to May 1974
May 1972 to March 1973	April 1975 to April 1976
September 1976 to February 1977	October 1984 to May 1985
April 1982 to June 1983	May 1988 to May 1989
August 1986 to February 1988	September 1995 to March 1996
April 1991 to July 1992	July 1998 to December 1998
August 1994 to March 1995	
April 1997 to April 1998	

[a]An El Niño (La Niña) event is defined as a phase of at least 6 consecutive months in which the 5-month running mean of SSTA in the NINO3.4 region exceeds (or remains below) 0.5°C (−0.5°C). The reference period for the SSTA is 1951–1980.

mean total precipitation amount in Central Brazil (Figure 9g). The GISS model fails to reproduce this SE Brazil precipitation anomaly and generally lacks much of the spatial coherence of the ENSO-related precipitation signal, apparent both in NCEP-NCAR reanalysis and ECHAM simulations.

4. Climatic Controls on $\delta^{18}O$

[27] Many studies have demonstrated the seasonal dependence of $\delta^{18}O$ composition on precipitation amount at low latitudes [e.g., *Rozanski and Araguás-Araguás*, 1995; *Araguás-Araguás et al.*, 1998; *García et al.*, 1998; *Aravena et al.*, 1999]. Since we are more interested in relationships on interannual and longer timescales, all analyses in this and the following sections are based on anomalies, with the seasonal cycle removed by subtracting the long-term monthly mean from individual monthly values.

4.1. Temperature

[28] Figure 10 shows the correlation between monthly anomalies of $\delta^{18}O$ in precipitation and temperature in each grid box. The only physically meaningful relationship between temperature and $\delta^{18}O$ involves a positive correlation [*Dansgaard*, 1964]. In the observational data, such a positive correlation clearly dominates over the continents, except over southern South America (Figure 10d). Significant positive correlations, however, are limited to the Amazon basin, southern Brazil, and the southeastern United States. The ECHAM simulations (Figures 11a and 11b) show a strong land-sea contrast in their correlation field, which, although confirmed to some extent by observations, seems to indicate a stronger influence of the prescribed SST over the oceans than over land, as compared to the GISS model. The GISS model on the other hand, is unable to reproduce the observed significant positive correlation over tropical South America. This positive relationship between temperature and $\delta^{18}O$ anomalies seems to support the notion of a temperature influence on the $\delta^{18}O$ composition of precipitation at interannual and longer timescales [*Thompson et al.*, 2000]. However, warm (cold) anomalies over tropical South America tend to coincide with dry (wet) episodes, and the significant relationship in Figure 10 might partly reflect the correlation between the two climatic controls, temperature and precipitation. The inspection of the temporal slope of the interannual $\delta^{18}O$-temperature relationship based on the IAEA stations with a significant correlation (not shown) renders further support for this notion. The only station in midlatitudes with a significant correlation (Cape Hatteras) features an interannual slope of 0.43‰/°C, somewhat lower than the 0.6‰/°C commonly used in mid- and high-latitude studies [e.g., *Rozanski et al.*, 1992]. The tropical stations in the Amazon and southern Brazil on the other hand, which also indicated a significant $\delta^{18}O$ dependence on temperature on interannual timescales, feature unusually high slopes of 1.64‰/°C (Belem), 1.58‰/°C (Brasilia), 1.28‰/°C (Manaus), and 1.13‰/°C (Sao Gabriel), respectively.

4.2. Precipitation Amount

[29] Precipitation anomalies are significantly negatively correlated with the $\delta^{18}O$ values on interannual timescales throughout the tropical Americas (Figure 11), in accordance with the classic "amount effect" theory [*Dansgaard*, 1964]. This relationship is apparent in the correlation field with the IAEA network (Figure 11d), where the vast majority of the stations feature a significant correlation. All three simulations confirm this result and show significant correlations everywhere, except for the most arid zones, influenced by the subtropical anticyclones. All stations that featured a significant correlation of their $\delta^{18}O$ anomalies with temperature, are also significantly correlated with the precipitation amount. In the interior of tropical South America, however, the relationship is insignificant at several stations, which might be caused by poor data quality or short time series of the IAEA data or reflect evapotranspiration processes, which tend to mask the correlation between $\delta^{18}O$ and the precipitation amount over the Amazon basin [e.g., *Gonfiantini*, 1985]. The interannual temporal slope of the $\delta^{18}O$-precipitation relationship (not shown) shows a wide range but the majority cluster between −0.4 and −0.8‰/100 mm. Much of the spatial variability of the temporal slope can be attributed to the different geographic positions of the IAEA stations. High elevation inland locations such as the Andean stations La Paz (4071 m: −1.82‰/100 mm), Izobamba (3058 m: −1.12‰/100 mm), Bogota (2547 m: −3.50‰/100 mm) or Salta (1187m: −1.61‰/100 mm),

Figure 9. (opposite) Difference in precipitation (in percent) between El Niño and La Niña periods for DJF (top row) and JJA (third row from top) based on: (column 1) NCEP-NCAR reanalysis data (1951–1998); (column 2) ECHAM-4 T30 (1951–1994); (column 3) ECHAM-4 T106 (1979–1998); and (column 4) GISS II (1980–1997). Regions with less than 1 mm precipitation (long-term average) are shaded gray. Second (fourth) row show regions with precipitation that is significantly different at the 95% level between El Niño and La Niña periods during DJF (JJA) based on two-tailed Student's *t*-test. Regions with significantly higher precipitation during El Niño (La Niña) are shaded in dark (light) gray. Please note the color scheme; blue (red) colors denote increased (decreased) precipitation during El Niño periods.

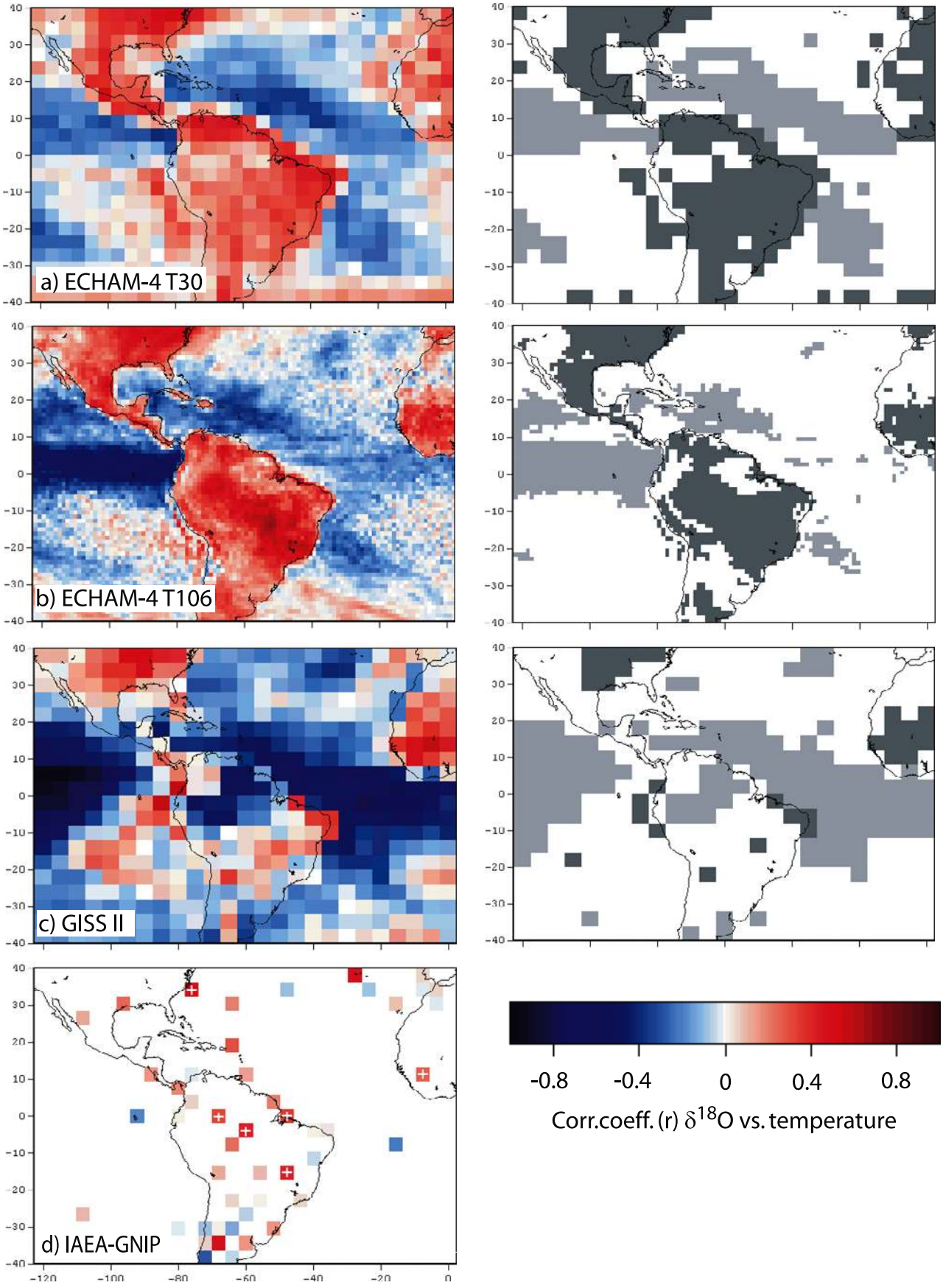
a) ECHAM-4 T30
b) ECHAM-4 T106
c) GISS II
d) IAEA-GNIP
-0.8
-0.4
0
0.4
0.8
Corr.coeff. (r) δ18O vs. temperature

feature a much steeper than average slope, while coastal lowland stations, e.g., Fortaleza (27 m: −0.19‰/100 mm), Salvador (45 m: −0.26‰/100 mm) and Ceara Mirim (8 m: −0.34‰/100 mm) are at the other end of the spectrum.

4.3. Moisture Source

[30] To investigate the influence of varying moisture sources (cf. Figure 7) to a local $\delta^{18}O$ signal, we first correlated the monthly $\delta^{18}O$ anomalies in each grid cell with the percent contribution anomaly of each source (Figure 12). Because the tagging capability was implemented in the control run of the ECHAM-4 model only (see Table 1), we here limit the discussion to the results from the GISS II simulation. To avoid spurious correlations in regions where a particular moisture source is of no relevance, we further limited the analysis to correlations over the grid cells that receive at least 5% of their annual mean precipitation from that particular source. A similar analysis has recently been presented on a global scale by *Cole et al.* [1999], although their simulation was based on a 8°lat. × 10°long. grid with the conventional GISS II topography, and a less detailed source region delineation in the tropics. Over the tropical oceans positive correlations dominate, which indicates that a higher amount of local (nonlocal) precipitation is associated with more enriched (depleted) $\delta^{18}O$ values. This result is to be expected and reflects the gradual rainout and increasingly depleted composition of water vapor along its trajectory. The farther from its evaporative source that water vapor contributes to local precipitation, the more negative is therefore the correlation with the local $\delta^{18}O$ signal. The major exception to this rule occurs over the Amazon basin, where the local source contribution is negatively correlated with the $\delta^{18}O$ composition of precipitation (Figure 12e). This inverse relationship may reflect the recycling of already depleted precipitation over the tropical continent, leading to more negative $\delta^{18}O$ values than precipitation originating from moisture evaporating upstream over the tropical Atlantic. Indeed, the correlation of $\delta^{18}O$ anomalies over the Amazon basin with moisture contribution from the tropical Atlantic is positive over the entire northern part of the basin (Figure 12f). It appears that considering the effects of continental moisture recycling is crucial to understanding the isotopic signal in areas where recycled water amounts to a substantial part of the total precipitation [e.g., *Koster et al.*, 1993].

[31] Another way of looking at the influence of different moisture sources on a grid cell's $\delta^{18}O$ signal is to separate the monthly $\delta^{18}O$, which represents a mix of all source regions contributing to precipitation at the given grid box and month, into its regional source components. Figure 13 shows the simulated annual mean precipitation-weighted $\delta^{18}O$ composition of precipitation over the tropical Americas, based on the ECHAM-4 T30 CTR simulation, for each of the moisture sources presented in Figure 1b. Again, the $\delta^{18}O$ signal is only plotted where a particular source contributes at least 5% to the annual mean precipitation. However, it should be kept in mind that the results for the GISS II model (Figure 12) are based on an 18-year integration using observed SST between 1980 and 1997, while the ECHAM-4 T30 results (Figure 13) are based on a 10-year control run with climatological SST. In addition, the source regions are slightly different between the two experiments as outlined in section 2 and Figure 1. Overall, the results from the ECHAM-4 T30 CTR simulation are consistent with the correlation analysis in Figure 12. Clearly, the $\delta^{18}O$ signal is the most enriched if it precipitates over the original source region, while a long transport distance leads to an increased depletion in heavy isotopes. Accordingly, the $\delta^{18}O$ composition of precipitation over a given grid cell varies significantly, depending on the precipitation source. Over the southern United States for example, the $\delta^{18}O$ value is most negative if precipitation originates over the equatorial Pacific (Figure 13d), while it is most enriched if the source is the North American continent itself (Figure 13a). Moisture evaporating over the equatorial and northern Atlantic (Figures 13c and 13f) and precipitating over the United States has an intermediate signature. A similar picture emerges over the tropical Andes, where values are most depleted if the precipitation originates from far upstream over the equatorial Atlantic (Figure 13f), consistent with the results from the GISS experiment. The enriched precipitation over the Andes originating from the South American continent itself, however (Figure 13e), shows the lack of realistic altitude and continentality effects in the ECHAM-4 T30 model, as discussed in section 3.4.

4.4. ENSO

[32] Since temperature, precipitation amount, and to some extent also moisture source contribution are all affected by ENSO, and they are at the same time major controlling factors on the stable isotopic content of precipitation, it is interesting to see if the $\delta^{18}O$ signal in precipitation shows a significant response to ENSO-related climatic changes as well [e.g., *Cole et al.*, 1993]. The evidence based on the IAEA observational network (Figure 14d) indicates that the $\delta^{18}O$ in precipitation is significantly more enriched (depleted) during the warm (cold) phase of ENSO over tropical South America. Over the north Atlantic, the eastern equatorial Pacific and southern South America the signal is reversed, that is, more enriched (depleted) values are related to La Niña (El Niño) periods, which is consistent with other observations [e.g., *Bird*, 1988], although none of the correlations reach the 95% confidence level. All three model simulations are able to capture this general pattern, which is quite surprising, given the fact that their capability of correctly assessing the ENSO-related precipitation anomalies seemed somewhat limited (Figure 9). Notwithstanding, the experiments all feature significant positive correlations

Figure 10. (opposite) Correlation between monthly anomalies in $\delta^{18}O$ of precipitation and surface temperature in each grid box. Left column shows correlation pattern, right column shows regions with significant positive (negative) correlation at the 95% confidence level in dark (light) gray shading. (a) ECHAM-4 T30 (1950–1994), (b) ECHAM-4 T106 (1979–1998), (c) GISS II (1980–1997), and (d) IAEA observational data, with significant correlations indicated by white cross. Reference period for anomalies is entire length of record, except for ECHAM-4 T30 where it is 1961–1990.

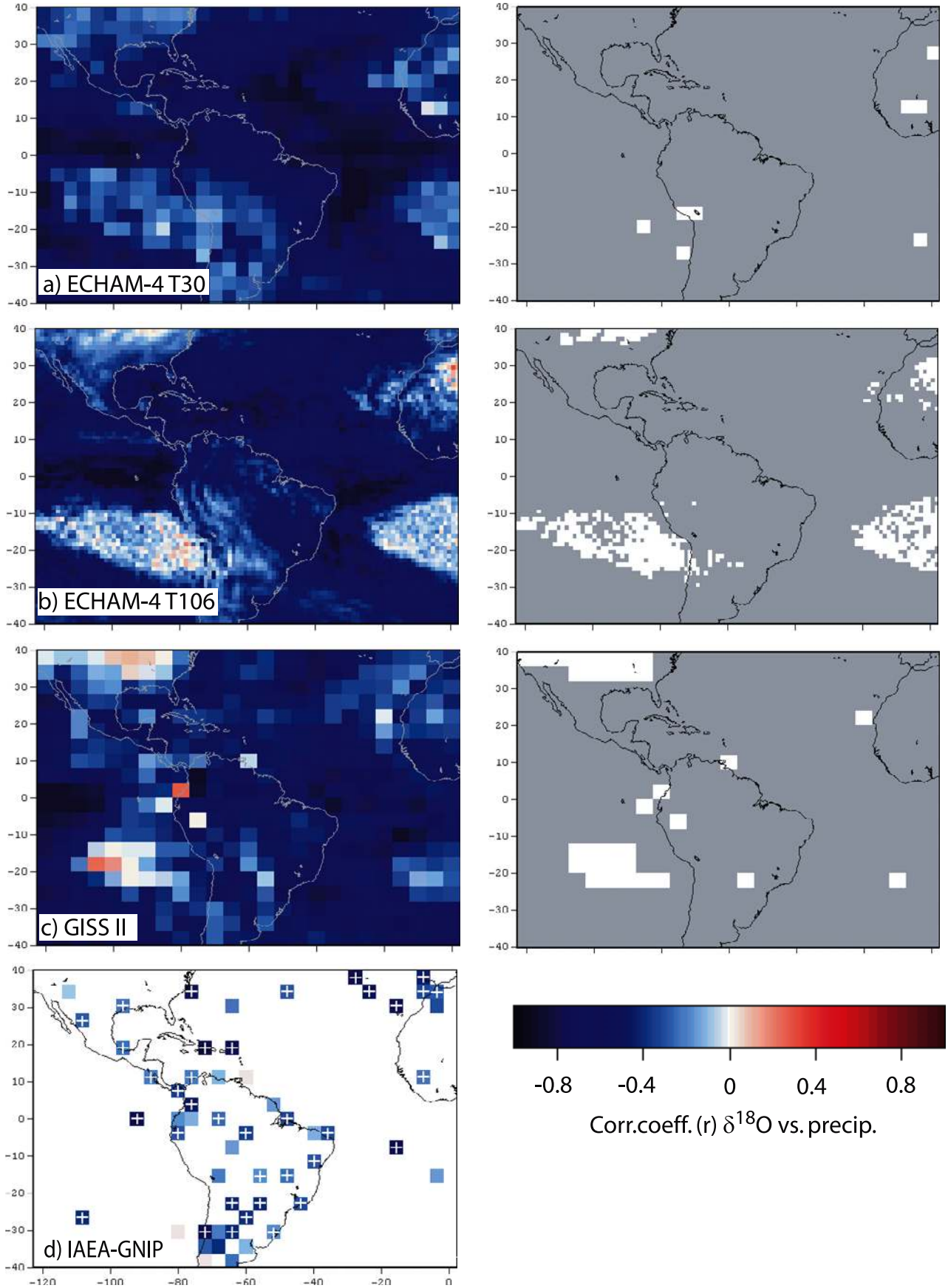

Figure 11. As in Figure 10 but for correlation between monthly anomalies of $\delta^{18}O$ in precipitation and precipitation amount in each grid box.

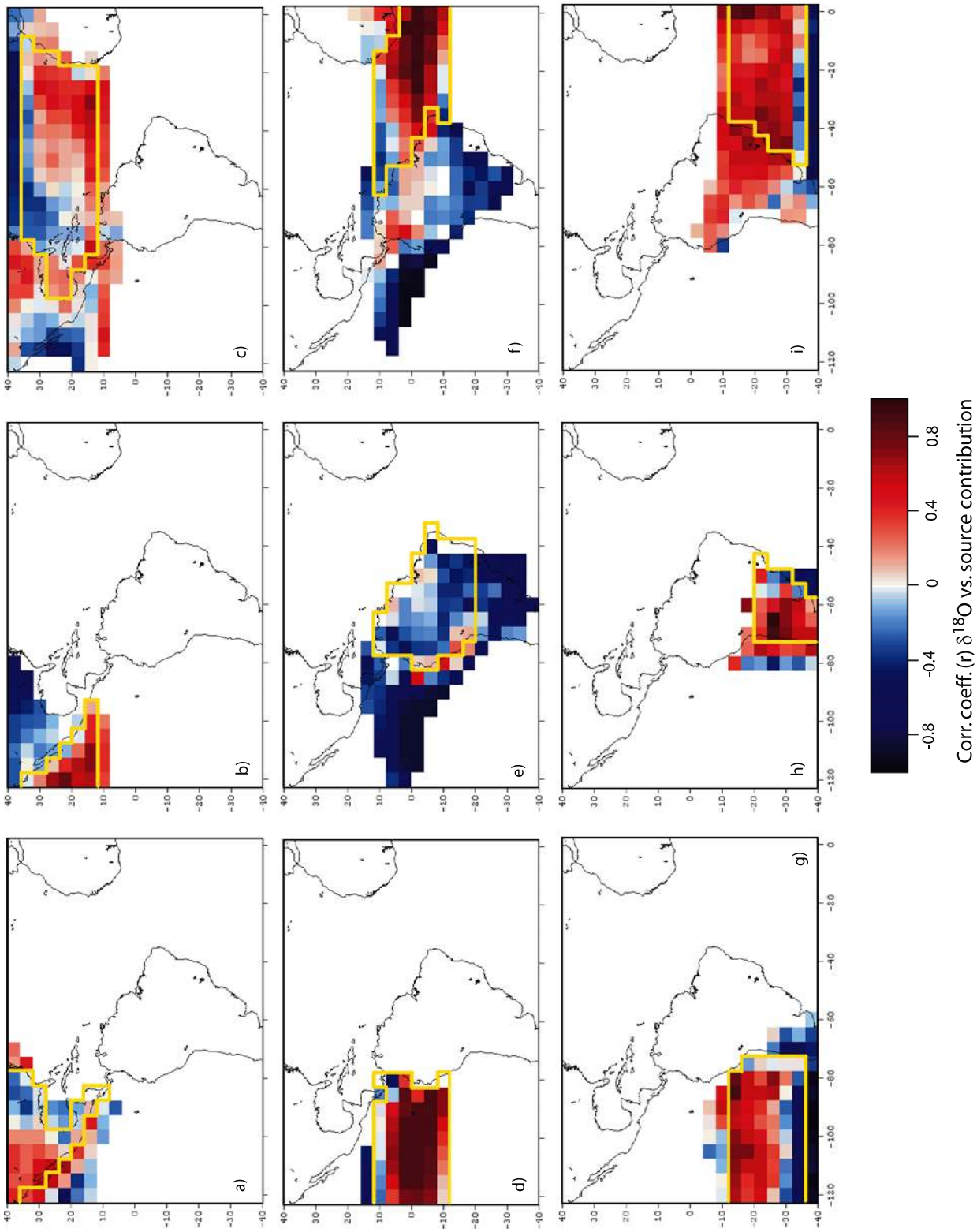

Figure 12. Correlation between monthly anomalies of $\delta^{18}O$ in precipitation in each grid cell and the percent contribution anomaly of each source in the GISS II model (1980–1997). Moisture sources are the same as in Figures 1 and 7 and outlined in yellow for clarity. Correlations are only shown for grid cells where the respective source contributes >5% to the annual precipitation total. Reference period for anomalies is entire length of record.

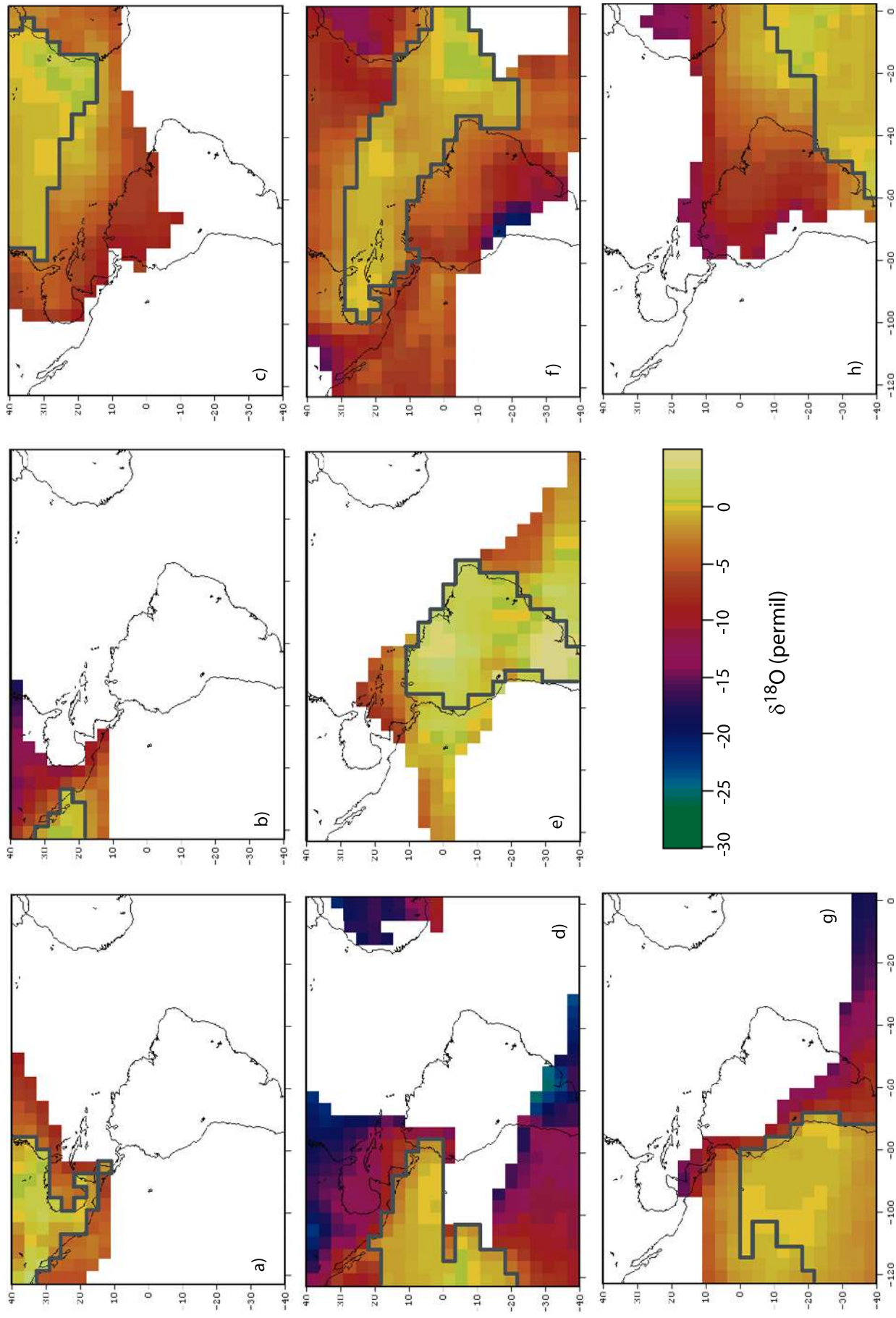
a)
b)
c)
d)
e)
f)
g)
h)
δ18O (permil)
0
-5
-10
-15
-20
-25
-30

over tropical South America extending into the tropical Atlantic, and negative correlations over the eastern equatorial Pacific, the southeastern US (significant in the ECHAM-4 T30 simulation only) and southern South America (insignificant in all experiments), all in accordance with the observations.

[33] Obviously the change in the $\delta^{18}O$ values in the tropics associated with ENSO is primarily a response to changes in precipitation rather than temperature. The ENSO-related temperature signal is of the same sign over the tropical continent and the eastern Pacific (see Figure 8), while both precipitation and $\delta^{18}O$ show a distinct dipole pattern with increased precipitation (depleted $\delta^{18}O$ values) over the eastern equatorial Pacific and decreased precipitation (enriched $\delta^{18}O$ values) over tropical South America during the ENSO warm phase (Figures 9 and 14). The shift in the Walker circulation during ENSO is the most likely cause to explain this dipole pattern seen in both the observed and modeled precipitation and $\delta^{18}O$ fields. In the midlatitudes (United States and southern South America), the ENSO-related controls on $\delta^{18}O$ are not as straightforward, because the observed depletion of $\delta^{18}O$ in precipitation during El Niño events could be caused both by lower temperatures and/or increased precipitation.

5. Summary and Conclusions

[34] The comparison between the different experiments using the ECHAM-4 and GISS II AGCMs is encouraging. Both models capture the essential features of surface climate (temperature and precipitation) over the tropical Americas in terms of both their spatial and temporal (seasonal to interannual) characteristics. The spatial $\delta^{18}O$ distribution over the tropical Americas is improved when a higher-resolution model is used (ECHAM-4 T106), or a low-resolution model is adjusted to provide a more realistic Andean topography (GISS-II). This results in a more accurate simulation of both surface temperature and $\delta^{18}O$ over the Andes and thus an altitude effect comparable to observations. Nonetheless, the continentality effect over the Amazon basin is underestimated in the ECHAM experiments, probably because the simulated precipitation is too low over the eastern part of the basin. Unfortunately, the lack of a dense observational stable isotope network precludes a detailed test of the model performance in some parts of the tropical Americas.

[35] On interannual timescales, ENSO is the most important factor causing climatic fluctuations over the tropical Americas. The surface temperature change associated with ENSO is nicely reproduced in both models. The major ENSO-induced precipitation anomalies, such as the precipitation increase over the eastern tropical Pacific or the decrease over tropical South America, are also correctly simulated, but considerable discrepancies occur in the precipitation fields on a regional scale.

[36] Anomalies of $\delta^{18}O$ are significantly negatively correlated with anomalies in the precipitation amount throughout almost the entire region, except for the large subsidence areas of the dry subtropics. This is consistent with the rather short and sparse records available from IAEA-GNIP. Over the continents, $\delta^{18}O$ anomalies are positively correlated with surface temperature. However, correlations are much weaker than for precipitation amount and significant in limited regions such as the Amazon basin only. While the ECHAM model is able to simulate this relationship suggested by the IAEA-GNIP observational data, the GISS model fails to reproduce the positive correlation over tropical South America. Both models accurately portray the water vapor transport and the gradual rainout and increasingly depleted composition of water vapor along its trajectory. The farther from its source that water vapor contributes to local precipitation, the more negative is the correlation with the local $\delta^{18}O$ signal.

[37] Finally, the ENSO-related variability of $\delta^{18}O$ in precipitation is almost identical in all simulations and seems to accurately portray what is known based on observational evidence. The pronounced east-west pattern with negative $\delta^{18}O$-NINO3.4 correlations over the eastern tropical Pacific and positive correlations over the tropical South American continent resembles the precipitation response to ENSO. The temperature response on the other hand is of the same sign over both the Pacific Ocean and the tropical continent. This indicates that the ENSO-signal in $\delta^{18}O$ may be caused by an amount effect dominating over a simultaneous temperature effect. Otherwise, one would expect to see a coherent stable isotopic response of the same sign throughout the tropics.

[38] Overall our results indicate that, in the tropical Americas, $\delta^{18}O$ is most likely not a good indicator of just one climatic variable, such as surface temperature or precipitation amount at the site. Clearly, the stable isotopic composition of precipitation is influenced by several factors, which include precipitation amount, temperature, source region contribution, and therefore also the atmospheric circulation. *Cole et al.* [1999] recently reached similar conclusions in their global modeling study and argued that a complex combination of different factors influence the $\delta^{18}O$ signal on different timescales. If this is indeed the case, then it is not possible to attribute the $\delta^{18}O$ signal preserved in ancient precipitation records such as ice cores to a single climatic variable. A more integrated view of climate variability, focusing on the dominant modes such as ENSO, may thus be more helpful when interpreting the $\delta^{18}O$ signal in precipitation of ancient

Figure 13. (opposite) Annual mean $\delta^{18}O$ signature of precipitation (in permil) associated with different moisture sources in the ECHAM-4 T30 CTR simulation. (a) North America (source region A in Figure 1), (b) tropical North Pacific (B), (c) tropical North Atlantic (C), (d) equatorial Pacific (D), (e) South America (E), (f) equatorial Atlantic (F), (g) tropical South Pacific (G), and (h) tropical South Atlantic (I). Annual mean $\delta^{18}O$ value is precipitation-weighted average of the monthly mean data and only plotted where respective source contributes >5% to annual precipitation. Source regions are outlined in gray for clarity.

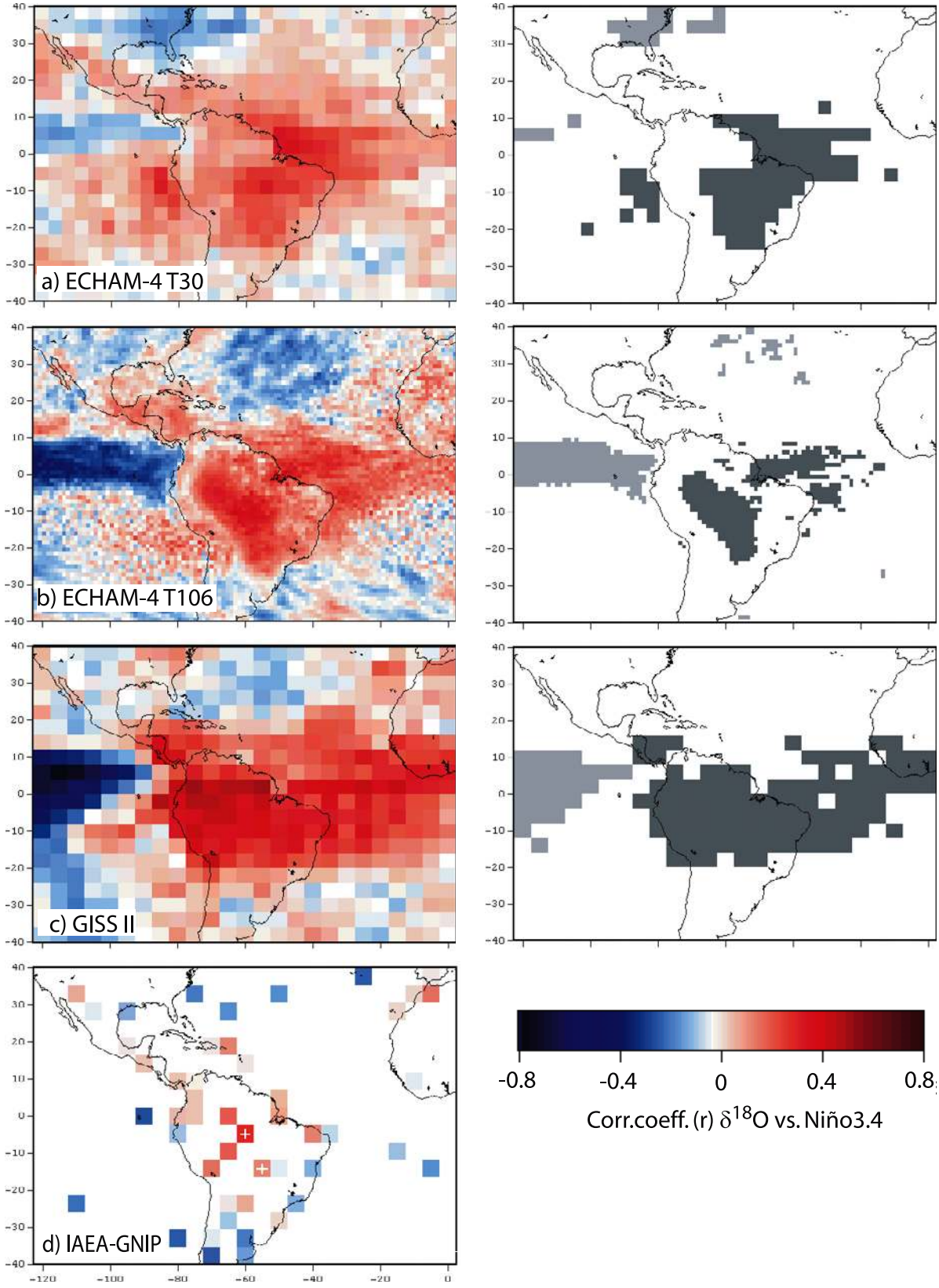

Figure 14. Correlation between NINO3.4 SSTA and monthly anomalies of $\delta^{18}O$ in precipitation. Left column shows correlation pattern, right column shows regions with significant positive (negative) correlation at the 95% confidence level in dark (light) gray shading. (a) ECHAM-4 T30 (1950–1994), (b) ECHAM-4 T106 (1979–1998), (c) GISS II (1980–1997), and (d) IAEA observational data, with significant correlations indicated by white cross. Reference period for anomalies is entire length of record, except for ECHAM-4 T30, where it is 1961–1990.

paleorecords, rather than trying to disentangle the competing effects of precipitation amount, temperature, and moisture source contribution.

[39] **Acknowledgments.** We are grateful for the comments by Gilles Delaygue and Chris Charles on the GISS II isotopic tracer setup. Eric Steig and an anonymous reviewer provided inspiring comments, which helped to improve our manuscript. Observational stable isotope records were obtained from the International Atomic Energy Agency-Global Network for Isotopes in Precipitation (IAEA-GNIP) database. NCEP-NCAR reanalysis data were provided by the NOAA Climate Diagnostics Center. GTOPO 30 data are distributed by the EROS Data Center Distributed Active Archive Center (EDC DAAC). ECHAM simulations were performed with support of the German Climate Computing Center (DKRZ) in Hamburg, Germany. This study was funded by US-NSF grant ATM-9909201 and the US Department of Energy.

References

Aceituno, P., On the functioning of the Southern Oscillation in the South American sector, part I, Surface climate, *Mon. Weather Rev.*, *116*, 505–524, 1988.

Aceituno, P., On the functioning of the Southern Oscillation in the South American Sector, part II, Upper-air circulation, *J. Clim.*, *2*, 341–355, 1989.

Araguás-Araguás, L., K. Froehlich, and K. Rozanski, Stable isotope composition of precipitation over Southeast Asia, *J. Geophys. Res.*, *103*, 28,721–28,742, 1998.

Aravena, R., O. Suzuki, H. Peña, A. Pollastri, H. Fuenzalida, and A. Grilli, Isotopic composition and origin of the precipitation in Northern Chile, *Appl. Geochem.*, *14*, 411–422, 1999.

Armengaud, A., R. D. Koster, J. Jouzel, and P. Ciais, Deuterium excess in Greenland snow: Analysis with simple and complex models, *J. Geophys. Res.*, *103*, 8947–8953, 1998.

Bendix, J., Precipitation dynamics in Ecuador and northern Peru during the 1991/92 El Niño: A remote sensing perspective, *Int. J. Remote Sens.*, *21*, 533–548, 2000.

Berri, G. J., and J. Inzunza, The effect of the low-level jet on the poleward water vapour transport in the central region of South America, *Atmos. Environ.*, *27A*, 335–341, 1993.

Bird, M., Isotopically depleted rainfall and El Niño, *Nature*, *331*, 489–490, 1988.

Bradley, R. S., H. F. Diaz, G. N. Kiladis, and J. K. Eischeid, ENSO signals in continental temperature and precipitation records, *Nature*, *327*, 497–501, 1987.

Charles, C. D., J. Rind, J. Jouzel, R. D. Koster, and R. G. Fairbanks, Glacial-interglacial changes in moisture sources for Greenland: Influences on the ice core record of climate, *Science*, *263*, 508–511, 1994.

Cole, J. E., D. Rind, and R. G. Fairbanks, Isotopic responses to interannual climate variability simulated by an atmospheric general circulation model, *Quat. Sci. Rev.*, *12*, 387–406, 1993.

Cole, J. E., D. Rind, R. S. Webb, J. Jouzel, and R. Healy, Climatic controls on interannual variability of precipitation $\delta^{18}O$: Simulated influence of temperature, precipitation amount, and vapor source region, *J. Geophys. Res.*, *104*, 14,223–14,235, 1999.

Costa, M. H., and J. A. Foley, A comparison of precipitation datasets for the Amazon basin, *Geophys. Res. Lett.*, *25*, 155–158, 1998.

Costa, M. H., and J. A. Foley, Trends in the hydrologic cycle of the Amazon basin, *J. Geophys. Res.*, *104*, 14,189–14,198, 1999.

Curtis, S., and S. Hastenrath, Trends of upper-air circulation and water vapour over equatorial South America and adjacent oceans, *Int. J. Climatol.*, *19*, 863–876, 1999.

Dansgaard, W., Stable isotopes in precipitation, *Tellus*, *16*, 436–468, 1964.

Deser, C., and J. M. Wallace, Large-scale atmospheric circulation features of warm and cold episodes in the tropical Pacific, *J. Clim.*, *3*, 1254–1281, 1990.

Diaz, A. F., C. D. Studzinski, and C. R. Mechoso, Relationships between precipitation anomalies in Uruguay and southern Brazil and sea surface temperature in the Pacific and Atlantic oceans, *J. Clim.*, *11*, 251–271, 1998.

Eltahir, A. B., and R. L. Bras, Precipitation recycling in the Amazon basin, *Q. J. R. Meteorol. Soc.*, *120*, 861–880, 1994.

Garcia, M., F. Villalba, L. Araguas-Araguas, and K. Rozanski, The role of atmospheric circulation patterns in controlling the regional distribution of stable isotope contents in precipitation: Preliminary results from two transects in the Ecuadorian Andes, in *Isotope Techniques in the Study of Environmental Change*, *Proc. Ser. IAEA, IAEA-SM-349/7*, pp. 127–140, Int. At. Energy Agency, Vienna, 1998.

Garreaud, R. D., and P. Aceituno, Interannual rainfall variability over the South American Altiplano, *J. Clim.*, *14*, 2779–2789, 2001.

Garreaud, R. D., and D. S. Battisti, Interannual (ENSO) and interdecadal (ENSO-like) variability in the southern hemisphere tropospheric circulation, *J. Clim.*, *12*, 2113–2123, 1999.

Garreaud, R. D., M. Vuille, and A. Clement, The climate of the Altiplano: Observed modern conditions and mechanisms of past climate change, *Palaeogeogr. Palaeoclimatol. Palaeoecol.*, in press, 2003.

Giannini, A., Y. Kushnir, and M. A. Cane, Interannual variability of Carribean rainfall, ENSO and the Atlantic Ocean, *J. Clim.*, *13*, 297–311, 2000.

Goldberg, R. A., G. Tisnado, and R. A. Scofield, Characteristics of extreme rainfall events in Northwestern Peru during the 1982–1983 El Niño period, *J. Geophys. Res.*, *92*, 14,225–14,241, 1987.

Gonfiantini, R., On the isotopic composition of precipitation in tropical stations, *Acta Amazonica*, *15*, 121–139, 1985.

Gonfiantini, R., M.-A. Roche, J.-C. Olivry, J.-C. Fontes, and G. M. Zuppi, The altitude effect on the isotopic composition of tropical rains, *Chem. Geol.*, *181*, 147–167, 2001.

Grabczak, J., J. Niewodniczanski, and K. Rozanski, Isotope stratification in high mountain glaciers: Examples from the Peruvian Andes and Himalaya, *J. Glaciol.*, *29*, 417–424, 1983.

Grimm, A. M., S. E. Ferraz, and J. Gomes, Precipitation anomalies in Southern Brazil associated with El Nino and La Nina events, *J. Clim.*, *11*, 2863–2880, 1998.

Grimm, A. M., V. R. Barros, and M. E. Doyle, Climate variability in Southern South America associated with El Nino and La Nina events, *J. Clim.*, *13*, 35–58, 2000.

Grootes, P. M., M. Stuiver, L. G. Thompson, and E. Mosley-Thompson, Oxygen isotope changes in tropical ice, Quelccaya, Peru, *J. Geophys. Res.*, *94*, 1187–1194, 1989.

Halpert, M. S., and C. F. Ropelewski, Surface temperature patterns associated with the Southern Oscillation, *J. Clim.*, *5*, 577–593, 1992.

Hansen, J., G. Russel, D. Rind, P. Stone, A. Lacis, S. Lebedeff, R. Ruedy, and L. Travis, Efficient three-dimensional global models for climate studies: Models I and II, *Mon. Weather Rev.*, *111*, 609–662, 1983.

Hansen, J., et al., Forcings and chaos in interannual to decadal climate change, *J. Geophys. Res.*, *102*, 25,679–25,720, 1997.

Hastenrath, S., Diagnostics and prediction of anomalous river discharge in Northern South America, *J. Clim.*, *3*, 1080–1096, 1990.

Hoffmann, G., and M. Heimann, Water isotope modeling in the Asian monsoon region, *Quat. Int.*, *37*, 115–128, 1997.

Hoffmann, G., M. Werner, and M. Heimann, Water isotope module of the ECHAM atmospheric general circulation model: A study on timescales from days to several years, *J. Geophys. Res.*, *103*, 16,871–16,896, 1998.

Hoffmann, G., J. Jouzel, and V. Masson, Stable water isotopes in atmospheric general circulation models, *Hydrol. Processes*, *14*, 1385–1406, 2000.

Hoffmann, G., J. Jouzel, and S. Johnsen, Deuterium excess record from central Greenland over the last millenium: Hints of a North Atlantic signal during the Little Ice Age, *J. Geophys. Res.*, *106*, 14,265–14,274, 2001.

Horel, J. D., and A. G. Cornejo-Garrido, Convection along the coast of northern Peru during 1983: Spatial and temporal variation of clouds and rainfall, *Mon. Weather Rev.*, *114*, 2091–2105, 1986.

Joussaume, S., and J. Jouzel, Paleoclimatic tracers: An investigation using an Atmospheric Circulation model under Ice Age conditions, 2, Water isotopes, *J. Geophys. Res.*, *98*, 2807–2830, 1993.

Jouzel, J., G. L. Russell, R. J. Suozzo, R. D. Koster, J. W. C. White, and W. S. Broecker, Simulations of the HDO and $H_2{}^{18}O$ atmospheric cycles using the NASA-GISS general circulation model: The seasonal cycle for present day conditions, *J. Geophys. Res.*, *92*, 14,739–14,760, 1987.

Jouzel, J., R. D. Koster, R. J. Suozzo, L. Russell, J. W. C. White, and W. S. Broecker, Simulations of the HDO and $H_2{}^{18}O$ atmospheric cycles using the NASA GISS General Circulation Model: Sensitivity experiments for present-day conditions, *J. Geophys. Res.*, *96*, 7495–7507, 1991.

Jouzel, J., R. Koster, and S. Joussaume, Climate reconstruction from water isotopes: What do we learn from isotopic models?, *NATO ASI Ser.*, *1*(41), 213–241, 1996.

Jouzel, J., G. Hoffmann, R. D. Koster, and V. Masson, Water isotopes in precipitation: Data/model comparison for present-day and past climates, *Quat. Sci. Rev.*, *19*, 363–379, 2000.

Kalnay, E., et al., The NCEP/NCAR 40-year reanalysis project, *Bull. Am. Meteorol. Soc.*, *77*, 437–471, 1996.

Kiladis, G. N., and H. Diaz, Global climatic anomalies associated with extremes in the Southern Oscillation, *J. Clim.*, *2*, 1069–1090, 1989.

Koster, R. D., J. Jouzel, R. Suozzo, and G. Russel, Global sources of local precipitation as determined by the NASA/GISS GCM, *Geophys. Res. Lett.*, *13*, 121–124, 1986.

Koster, R. D., P. de Valpine, and J. Jouzel, Continental water recycling and $H_2{}^{18}O$ concentrations, *Geophys. Res. Lett.*, *20*, 2215–2218, 1993.
Krinner, G., C. Genthon, and J. Jouzel, GCM analysis of local influences on ice core delta signals, *Geophys. Res. Lett.*, *24*, 2825–2828, 1997.
Liebmann, B., J. A. Marengo, J. D. Glick, V. E. Kousky, I. C. Wainer, and O. Massambani, A comparison of rainfall, outgoing longwave radiation and divergence over the Amazon basin, *J. Clim.*, *11*, 2898–2909, 1998.
Mo, K. C., and R. W. Higgins, The Pacific-South American modes and tropical convection during the southern hemisphere winter, *Mon. Weather Rev.*, *126*, 1581–1596, 1998.
Montecinos, A., A. Diaz, and P. Aceituno, Seasonal diagnostic and predictability of rainfall in subtropical South America based on tropical Pacific SST, *J. Clim.*, *13*, 746–758, 2000.
Montroy, D. L., Linear relation of central and eastern North American precipitation to tropical Pacific sea surface temperature anomalies, *J. Clim.*, *10*, 541–558, 1997.
Moron, V., A. Navarra, M. N. Ward, and E. Roeckner, Skill and reproducibility of seasonal rainfall patterns in the tropics in ECHAM-4 GCM simulations with prescribed SST, *Clim. Dyn.*, *14*, 83–100, 1998.
Nogués-Paegele, J., and K. C. Mo, Alternating wet and dry conditions over South America during summer, *Mon. Weather Rev.*, *125*, 279–291, 1997.
Pisciottano, G., A. Diaz, G. Cazes, and C. R. Mechoso, El Niño-Southern Oscillation impact on rainfall in Uruguay, *J. Clim.*, *7*, 1286–1302, 1994.
Poveda, G., and O. J. Mesa, Feedbacks between hydrological processes in tropical South America and large-scale ocean-atmospheric phenomena, *J. Clim.*, *10*, 2690–2702, 1997.
Rao, V. B., I. F. A. Cavalcanti, and K. Hada, Annual variation of rainfall over Brazil and water vapor characteristics over South America, *J. Geophys. Res.*, *101*, 26,539–26,551, 1996.
Roeckner, E., K. Arpe, L. Bengtsson, M. Christoph, M. Claussen, L. Duemenil, M. Esch, M. Giorgetta, U. Schlese, and U. Schulzweida, The Atmospheric General Circulation Model Echam-4: Model description and simulation of present-day climate, Max Planck Inst. for Meteorol., Hamburg, 1996.
Rogers, J. C., Precipitation variability over the Caribbean and the tropical Americas associated with the Southern Oscillation, *J. Clim.*, *1*, 172–182, 1988.
Ropelewski, C. F., and M. S. Halpert, Quantifying Southern Oscillation-precipitation relationships, *J. Clim.*, *9*, 1042–1059, 1996.
Rozanski, K., and L. Araguás-Araguás, Spatial and temporal variability of stable isotope composition of precipitation over the South American continent, *Bull. Inst. Fr. Etud. Andines*, *24*, 379–390, 1995.
Rozanski, K., L. Araguás-Araguás, and R. Gonfiantini, Relation between long-term trends of oxygen-18 isotope composition of precipitation and climate, *Science*, *258*, 981–985, 1992.
Rutllant, J., and H. Fuenzalida, Synoptic aspects of the central Chile rainfall variability associated with the Southern Oscillation, *Int. J. Climatol.*, *11*, 63–76, 1991.
Steig, E. J., P. M. Grootes, and M. Stuiver, Seasonal precipitation timing and ice core records, *Science*, *266*, 1885–1886, 1994.
Tapley, T. D., and P. R. Waylen, Spatial variability of annual precipitation and ENSO events in western Peru, *J. Hydrol. Sci.*, *35*, 429–446, 1990.
Thompson, L. G., E. Mosley-Thompson, J. F. Bolzan, and B. R. Koci, A 1500 year record of tropical precipitation in ice cores from the Quelccaya Ice Cap, Peru, *Science*, *229*, 971–973, 1985.
Thompson, L. G., E. Mosley-Thompson, M. E. Davis, P. N. Lin, K. A. Henderson, J. Cole-Dai, J. F. Bolzan, and K. B. Liu, Late glacial stage and holocene tropical ice core records from Huascaran, Peru, *Science*, *269*, 46–50, 1995.
Thompson, L. G., et al., A 25,000-year tropical climate history from Bolivian Ice cores, *Science*, *282*, 1858–1864, 1998.
Thompson, L. G., E. Mosley-Thompson, and K. Henderson, Ice-core palaeoclimate records in tropical South America since the Last Glacial Maximum, *J. Quat. Sci.*, *15*, 377–394, 2000.
Trenberth, K., The definition of El Niño, *Bull. Am. Meteorol. Soc.*, *78*, 2771–2777, 1997.
Victoria, R. L., L. A. Martinelli, J. Mortatti, and J. Richey, Mechanisms of water recycling in the Amazon basin: Isotopic insights, *Ambio*, *20*, 384–387, 1991.
Vuille, M., Atmospheric circulation over the Bolivian Altiplano during dry and wet periods and extreme phases of the Southern Oscillation, *Int. J. Climatol.*, *19*, 1579–1600, 1999.
Vuille, M., D. R. Hardy, C. Braun, F. Keimig, and R. S. Bradley, Atmospheric circulation anomalies associated with 1996/97 summer precipitation events on Sajama ice cap, Bolivia, *J. Geophys. Res.*, *103*, 11,191–11,204, 1998.
Vuille, M., R. S. Bradley, and F. Keimig, Interannual climate variability in the Central Andes and its relation to tropical Pacific and Atlantic forcing, *J. Geophys. Res.*, *105*, 12,447–12,460, 2000a.
Vuille, M., R. S. Bradley, and F. Keimig, Climatic variability in the Andes of Ecuador and its relation to tropical Pacific and Atlantic sea surface temperature anomalies, *J. Clim.*, *13*, 2520–2535, 2000b.
Vuille, M., R. S. Bradley, R. Healy, M. Werner, D. R. Hardy, L. G. Thompson, and F. Keimig, Modeling $\delta^{18}O$ in precipitation over the tropical Americas, 2, Simulation of the stable isotope signal in Andean ice cores, *J. Geophys. Res.*, *108*, doi:10.1029/2001JD002039, in press, 2003.
Werner, M., and M. Heimann, Modeling interannual variability of water isotopes in Greenland and Antarctica, *J. Geophys. Res.*, *107*(D1), 4001, doi:10.1029/2001JD900253, 2002.
Werner, M., U. Mikolajewicz, M. Heimann, and G. Hoffmann, Borehole versus isotope temperatures on Greenland: Seasonality does matter, *Geophys. Res. Lett.*, *27*, 723–726, 2000a.
Werner, M., U. Mikolajewicz, G. Hoffmann, and M. Heimann, Possible changes of $\delta^{18}O$ in precipitation caused by a meltwater event in the North Atlantic, *J. Geophys. Res.*, *105*, 10,161–10,167, 2000b.
Werner, M., M. Heimann, and G. Hoffmann, Isotopic composition and origin of polar precipitation in present and glacial climate simulations, *Tellus Ser. B*, *53*, 53–71, 2001.

R. S. Bradley, F. Keimig, and M. Vuille, Climate System Research Center, Department of Geosciences, Morrill Science Center, University of Massachusetts, 611 North Pleasant Street, Amherst, MA 01003-9297, USA. (rbradley@geo.umass.edu; frank@geo.umass.edu; mathias@geo.umass.edu)

R. Healy, Woods Hole Oceanographic Institution, M.S. 8, 360 Woods Hole Road, Woods Hole, MA 02543, USA. (rhealy@whoi.edu)

M. Werner, Max Planck Institute for Biogeochemistry, P.O. Box 10 01 64, D-07701 Jena, Germany. (martin.werner@bgc-jena.mpg.de)